Peer-reviewed version available at *Fluids* **2016**, *1*, 30; doi:10.3390/fluids1030030

Article

MERIDIONAL AND ZONAL WAVENUMBER DEPENDENCE IN POTENTIAL VORTICITY FLUX IN ROSSBY WAVES

Sanjeeva Balasuriya

School of Mathematical Sciences, University of Adelaide, Adelaide SA 5005, Australia; sanjeevabalasuriya@yahoo.com

Abstract: Eddy-driven jets are of importance in the ocean and atmosphere, and to a first approximation are governed by Rossby wave dynamics. This study addresses the time-dependent flux of fluid and potential vorticity between such a jet and an adjacent eddy, with specific regard to determining zonal and meridional wavenumber dependence. The flux amplitude in wavenumber space is obtained, which is easily computable for a given jet geometry, speed and latitude, and which provides instant information on the wavenumbers of the Rossby waves which maximize the flux. This new tool enables the quick determination of which modes are most influential in imparting fluid exchange, which in the long term will homogenize the potential vorticity between the eddy and the jet. The results are validated by computing backward- and forward-time finite-time Lyapunov exponent fields, and also stable and unstable manifolds; the intermingling of these entities defines the region of chaotic transport between the eddy and the jet. The relationship of all of these to the time-varying transport flux between the eddy and the jet is carefully elucidated. The flux quantification presented here works for general time-dependence, whether or not lobes (intersection regions between stable and unstable manifolds) are present in the mixing region, and is therefore also easily computable for wave packets consisting of infinitely many wavenumbers.

Keywords: maximum flux; midlatitude cyclones; oceanic jets; chaotic transport

1. Introduction

Rossby waves are ubiquitous in the atmosphere and ocean, and arise from the earth's rotation and curvature [1,2]. Their structure is often associated with meandering jets of large horizontal extent, with mesoscale eddies within the meanders [3–7]. The term 'eddy' shall be used throughout this paper for these rotating structures as a generic identifier; in context, this could represent a 'vortex,' 'ring,' 'hurricane' or 'cyclone.' Classically, Rossby waves are obtained from the conservation of potential vorticity (PV), and a one-mode Rossby wave provides an excellent first-order approximation to meandering (eddy-driven) jets which have a dominant zonal and meridional spatial scale [1–3,8–10].

Crucial to the understanding of transport in the atmosphere and oceans is the presence of nominal transport barriers between coherent structures. These can be, for example, an oceanic front, the 'edge' of the Antarctic circumpolar vortex, the boundary between an eddy and an adjacent jet in the ocean, the boundary between a cyclone and a midlatitude jet, etc. One can think of these as *barriers* between mesoscale 'Lagrangian coherent structures' (LCSs), although there is confusion in this nomenclature since these barriers themselves are sometimes called LCSs [11]. These are only 'nominal' barriers in the sense that transport *does* occur across these, which makes it difficult to *define* exactly what the 'barrier' is. (This paper will offer some resolution to this issue under certain circumstances.) Nevertheless, understanding the interchange of fluid, PV, heat, salinity, nutrients, pollutants, energy, phytoplankton, etc, across these barriers is vital in evaluating the role of LCSs in the transport of these scalar quantities. The fact that the LCSs, and their boundaries, are themselves moving with time in arbitrary ways makes this proposition quite difficult. One diagnostic often used in oceanography and the atmospheric sciences to attempt to determine these barriers is

seeking strong ridges of finite-time Lyapunov exponent (FTLE) fields or the closely related finite-size Lyapunov exponent fields [12–24]. These barriers are also sought via many other methods, of which a nonexhaustive list is the hyperbolic LCS method of Haller [11], averaging applied to parcel trajectories [25–28], topological entropy of braids from intermingling Lagrangian trajectories [29,30], curves of least curvature deformation [31], exit/residence time fields [22,32], transport characterization using Perron-Frobenius operators [33–36], and a direct identification as stable/unstable manifolds [37–41]. A note of caution: *Eulerian* fields (e.g., instantaneous PV contours, Okubo-Weiss criterion, etc) are well-known to give an *incorrect* understanding of Lagrangian transport in genuinely unsteady flows [11], and thus shall be avoided here.

The *exact* conservation of PV imposes topological constraints which inhibit mixing between the jet and adjacent eddies [42,43]. In other words, the flow barrier between the coherent entities (the jet, and an adjacent eddy) remains impervious. Mixing is therefore associated with a PV flux generated via dynamically-relevant disturbances which *break* the conservation of PV. An early study by Pierrehumbert [3], in which a weak PV-conserving disturbance was added, demonstrated that chaotic mixing would result[1]. Many similar early studies, but with differing dynamical considerations [44–49], reached similar conclusions. In all these cases, the disturbance was *time-periodic*, and it is now well-established that in such instances, chaotic mixing is the *generic* expectation [12,41,50–52]. This line of study continues to be popular [20,53–55]. Time-aperiodicity is a different proposition, since it disallows the principal dynamical-systems tools for analyzing chaotic mixing used in the above mentioned studies: Poincaré maps which sample the flow at the period of the disturbance [46,47,49,51,54,55]. Nevertheless, there have been attempts to adapt the classical methodology for assessing transport in these situations [56–59]. These usually rely on quasi-periodicity and/or the possibility of identifying *lobes* of fluid in the chaotic region, whose areas are linked to transport. In realistic flows, however, very general time-variation is present [60, e.g.], for which a consistent theory would be valuable.

The intersections between dynamical-systems entities called *stable* and *unstable manifolds* is now well-known to be an instigator of mixing between coherent regions in fluid flows [12,41,46,61,62]. These can indeed be construed as the time-dependent 'barriers' discussed previously [39]. A recent restatement of their role in transport is that these are crucial flow separators in forward and backward time respectively [32]. Complicated intersections between stable and unstable manifolds at a particular instance in time identify regions in which large chaotic mixing is happening [49,51], but it must be borne in mind that in a genuinely unsteady flow, these entities are moving around with time. The regions bounded by intersections are called 'lobes' and are the basis of the classical lobe dynamics approaches to quantifying transport in fluids [49,51]. However, lobes need not exist in general time-aperiodic situations because it is possible for stable and unstable manifolds to *not* intersect; this is indeed generic when introducing dissipation into a geophysical flow [37,38,41]. Even if they do exist in a general time-varying flow, it is difficult to rationalize exactly *how* they transfer between, say, an eddy and the jet, and *when* the transfer happens.

Most transport studies which work with the Lagrangian trajectories focus on *fluid* flux. However, understanding scalar fluxes of many other quantities—such as heat, pollutant, energy, plankton and nutrients—is often of interest. From the geophysical perspective, the flux of the potential vorticity (PV) can also be considered important [23,56,63–67]. One contribution of the present article is to provide a method for quantifying both the fluid flux, *and* the PV flux, between an eddy and the jet as a *time-varying* entity, *without having the need to identify lobes*, or even for lobes to exist. This enables the determination of fluid/PV flux for disturbances which are not time-periodic, for example consisting of wave packets with zonal and meridional wavenumbers distributed either discretely or

[1] While the PV was conserved for both the dominant and the weak modes individually, it is only weakly conserved for their sum since the PV conservation equation is nonlinear.

continuously [68]. The computability of the flux in such situations is presented in Section 3.3. This new tool is anticipated to have applicability in other situations, for example in determining the future depletion of an eddy subject to wave packets with wavenumbers normally distributed around known stable values.

The second goal of this article is to specifically determine wavenumbers which provide extremal (maximal or minimal) chaotic mixing between a jet and an eddy, while being subject to Rossby wave dynamics. This is in the spirit of Farrell [69], who investigated wavenumbers which resulted in the most growth, and Barnes and Hartmann [7], who addressed the vorticity stirring power as a function of meridional wavenumber for the midlatitude eddy-driven jet; here the focus is on the most *eddy-jet transport*. These disturbances can arise from dynamical or physical considerations (e.g., the most stable modes [70]), wind-forcing on the ocean surface [60], or eddy diffusivity [63]). For a specific choice of wavenumbers, it is possible to *view* the resulting mixing [3,45], or to obtain measures of mixing [3], by numerically advecting many particles using either direct advection of parcel trajectories, or advection-diffusion of a tracer (e.g., PV) field. Having performed such a computation (for which a time-interval would need to be specified), tools such as the finite-time Lyaponuv exponent (FTLE) [9,12,32,54,71], mix-norm [72], effective diffusivity [73–75], network complexity [36] or topological entropy [29,30]—to name a few—can then be used to quantify mixing. Each such computation—for a specific chosen zonal and meridional wavenumber, and a chosen time-interval—would be tractable but relatively expensive. Using a method like this to search the parameter space of wavenumbers which maximizes eddy-jet transport is therefore prohibitive. A tool which can quickly identify the most and least influential wavenumbers for mixing would be highly useful. This study provides exactly that, and is able to tune it based on the geometry and dominant meandering jet and the local planetary parameter. The optimally-mixing zonal and meridional wavenumbers turn out to be distributed in a nonuniform and nonobvious manner, illustrating that this tool is indeed valuable.

The methods developed in this paper may allow for the investigation of many interesting issues. Could low energy excitations at optimally-mixing wavenumbers be used to maximize transport between an eddy and a jet? Alternatively, which geometry of meandering jet, and occurring at what latitudes, would be most effective at causing eddy-jet mixing due to the presence of white noise perturbations? Is it possible to determine wave packet disturbances which can cause an eddy to deplete very rapidly? If wavenumbers are gathered from an atmospheric or oceanic situation (by applying spatial Fourier transforms to observational data, say) at some instance in time, can this be used to predict eddy-jet transport into the future? Can the flux into/out of a midlatitude cyclone be determined from observed poleward momentum surges [8,76]?

This paper is organized as follows. Section 2.1 sets the stage by introducing the dominant Rossby wave which is associated with a meandering jet with flanking eddies. This is an exact solution to PV conservation dynamics, and reflects a situation in which there is *no* flux between the jet and an adjacent eddy. Section 2.2 defines how a fluid flux, and a PV flux, can be defined as time-varying quantities under the addition of an (approximately) dynamically-consistent Rossby wave, or Rossby wave packet. In the latter case, the system is genuinely time-aperiodic, necessitating the time-continuous definitions of the fluxes. This process in fact enables a definition of what the 'barrier' is in this situation in which there is actually transport across the so-called barrier. Appendix A provides a detailed discussion on the relationships between the flux as defined here, and classical transport quantifiers (lobe dynamics, width of chaotic layer, etc) which are applicable is less general situations. Section 3.2 provides the methodology for determining the zonal and meridional wavenumbers which maximize transport between the chosen eddy and the jet. The predictions obtained from this are validated by using both FTLEs and numerical computations of stable and unstable manifolds. Section 3.3 provides flux calculations for several wave packet situations, and Section 4 discusses avenues for future continuation of this work.

2. Materials and Methods

2.1. Rossby waves

A flow dominated by one Rossby wave can be represented by the streamfunction [3,6,10,12,54,57,69,77]

$$\psi_0'(x',y',t') = A' \sin\left[k_0'\left(x' - c_0' t'\right)\right] \sin\left[l_0' y'\right] \tag{1}$$

in which $c_0' = -\beta'/(k_0'^2 + l_0'^2)$, and (x', y') are the local eastward and northward coordinates, and (1) is an *exact* solution to the barotropic potential vorticity conservation equation [3], that is, the equation

$$\frac{\partial q_0'}{\partial t'} - \frac{\partial \psi_0'}{\partial y'}\frac{\partial q_0'}{\partial x'} + \frac{\partial \psi_0'}{\partial x'}\frac{\partial q_0'}{\partial y'} = 0\,, \tag{2}$$

where the barotropic potential vorticity (PV) is defined by

$$q_0'(x',y',t') = \nabla'^2\psi_0' + f_0' + \beta' y' = \frac{\partial^2 \psi_0'}{\partial x'^2} + \frac{\partial^2 \psi_0'}{\partial y'^2} + f_0' + \beta' y'\,. \tag{3}$$

The quantity f_0' is the nominal effect of the Coriolis parameter at the chosen latitude, and β', the linearized effect of its change when moving to nearby latuitudes. All variables with primes are dimensional, in contrast to nondimensional variables which shall be unprimed. Fluid parcel trajectories associated with this satisfy

$$\frac{dx'}{dt} = -\frac{\partial \psi_0'}{\partial y'} \quad , \quad \frac{dy'}{dt} = \frac{\partial \psi_0'}{\partial x'}\,. \tag{4}$$

Thus, (2) is an explicit statement that the PV is conserved following parcel trajectories of (4). Variables shall be changed to nondimensional ones which are stationary in the frame of reference of this wave. To this end, define nondimensional (unprimed) variables by

$$x = k_0'\left(x' - c_0' t'\right)\,,\; y = l_0' y'\,,\; t = A' k_0' l_0' t'\,,\; c = \frac{c_0'}{A' l_0'} = -\frac{\beta'}{A' l_0'\left(k_0'^2 + l_0'^2\right)}\,. \tag{5}$$

(It proves convenient to use the wavespeed c as the nondimensional parameter, noting that it encodes information about β'.) In these new variables, the parcel trajectories obey

$$\frac{dx}{dt} = -\frac{\partial \psi_0}{\partial y} \quad , \quad \frac{dy}{dt} = \frac{\partial \psi_0}{\partial x} \tag{6}$$

where the nondimensional streamfunction

$$\psi_0(x,y) = \sin x \sin y + cy\,, \tag{7}$$

incorporates both a scaling with respect to A' and a translation to the x frame of reference, and is now independent of time. For $-1 < c < 0$ (i.e., for the dimensional planetary parameter satisfying $0 < \beta' < A' l_0'(k_0'^2 + l_0'^2)$), the streamlines associated with (6) display a meandering jet with eddies on the side as shown in Figure 1. The jet travels eastward in this frame of reference, with the eddies rotating clockwise. If $0 < c < 1$, the picture is similar in spirit, but with all directions of flow reversed. If $|c| > 1$, there are no eddies (the meandering jet extends meridionally). The case $|c| = 1$ is a degenerate transition; the eddies present for $0 < |c| < 1$ shrink and disappear when $|c|$ exceeds 1. The case $c = 0$ consists of when the jet disappears; there are then square cells of alternating vorticity (the Taylor-Green flow [52]).

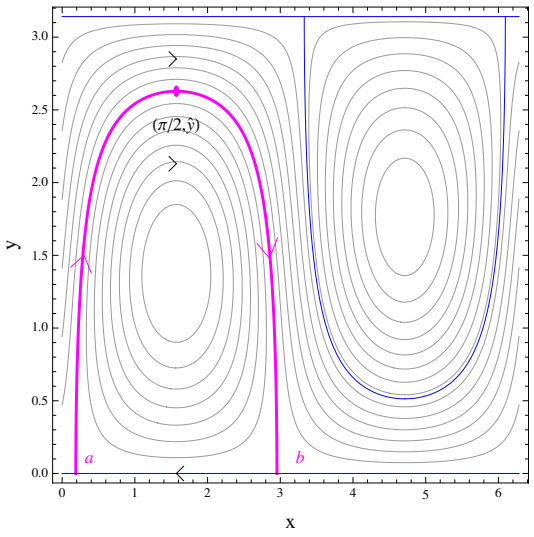

Figure 1. One-wave Rossby wave in the moving frame, with $-1 < c < 0$, where Γ [magenta curve] is the barrier between the chosen eddy and the jet.

Here, the generic situation of when $-1 < c < 0$ is the focus; Figure 1 has been produced with $c = -0.1868$ (associated with realistic parameters for a typical atmospheric midlatitude cyclone as reported by Oruba et al [9], to be discussed in detail later). The dimensional wavenumbers (k_0', l_0') are associated with the zonal and meridional reciprocal lengthscales of the eddy. In this case, the darker curves demarcate the boundaries between the jet and the eddies, across which there is no transport. This sort of qualitative behavior is common in many other dynamically-inspired or kinematic studies [44–47,55,78].

Before introducing a disturbance to this streamfunction, the PV conservation will also be written in nondimensional coordinates. Using the nondimensionalization

$$q_0(x,y) = \frac{q_0'(x',y',t')}{A'\left(k_0'^2 + l_0'^2\right)} \quad , \quad f_0 = \frac{f_0'}{A'\left(k_0'^2 + l_0'^2\right)} \,, \tag{8}$$

and defining the 'scaled Laplacian' by

$$\nabla_0^2 = \frac{k_0'^2}{\left(k_0'^2 + l_0'^2\right)} \frac{\partial^2}{\partial x^2} + \frac{l_0'^2}{\left(k_0'^2 + l_0'^2\right)} \frac{\partial^2}{\partial y^2} \,, \tag{9}$$

the nondimensional PV and streamfunctions possess the relationship

$$q_0(x,y) = \nabla_0^2 \psi(x,y) + f_0 - cy = -\sin x \sin y + f_0 - cy \,. \tag{10}$$

PV conservation is representible via

$$-\frac{\partial \psi_0}{\partial y}\frac{\partial q_0}{\partial x} + \frac{\partial \psi_0'}{\partial x'}\frac{\partial q_0'}{\partial y} = 0 \,. \tag{11}$$

The explicit time-dependence has dropped out in the PV, as it must, and consequently the time-derivative has disappeared from the PV conservation equation (11) in the new variables. This indeed represents the fact that q_0 is conserved by the flow (6). Comparing q_0 in (10) with (7), the flow of (6) is constrained to lie on curves of constant ψ_0, *or equivalently*, constant q_0. This is because of the direct functional relationship between ψ_0 and q_0, given by $q_0(x,y) = -\psi_0(x,y) + f_0$.

The goal is to capture the flux between the eddy in the southwest corner of Figure 1 and the main jet as a function of time, resulting from the presence of a dynamically relevant disturbance in the streamfunction. In other words, this is the flux across the heavy magenta curve in Figure 1, denoted Γ. This curve is the *stable manifold* of the saddle fixed point $\mathbf{b} = \left(\pi - \sin^{-1}(-c), 0\right)$ at the southeastern corner of the eddy. This is defined by the set of fluid parcels which in forward time approach $\mathbf{b}$. It turns out that this occurs exponentially slowly, since the velocity is zero at the saddle point. However, Γ is *also* the unstable manifold of the saddle fixed point $\mathbf{a} = \left(\sin^{-1}(-c), 0\right)$ at the southwestern corner of the eddy. That is, parcels on Γ approach $\mathbf{a}$ as $t \to -\infty$. Since Γ comprises a curve in which a stable manifold coincides with an unstable manifold, it is a *heteroclinic manifold* [51,79]. In this case, it is identifiable also as part of the level set $\psi_0 = 0$, or equivalently, $q_0 = f_0$.

The full (dimensional) flow will therefore consist of the dominant Rossby mode, plus a disturbation, i.e., fluid parcels will obey

$$\frac{dx'}{dt'} = -\frac{\partial \psi'}{\partial y'} \quad , \quad \frac{dy'}{dt'} = \frac{\partial \psi'}{\partial x'} \tag{12}$$

with streamfunction

$$\psi'(x', y', t') = \psi'_0(x', y', t') + \psi'_{\text{pert}}(x', y', t') \,. \tag{13}$$

The new PV will comply with (3), i.e.,

$$q'(x', y', t') = \nabla'^2 \psi' + f'_0 + \beta' y' = \frac{\partial^2 \psi'}{\partial x'^2} + \frac{\partial^2 \psi'}{\partial y'^2} + f'_0 + \beta' y' \,, \tag{14}$$

and will, at the least, *approximately* obey the conservation (11) with the 0-subscripts removed. In contrast to ψ'_0 in which the time-dependence disappears when converted according to (5), ψ' and q' will in general have arbitrary time-dependence. So for example it is *not* assumed that after the nondimensional transformation into the moving frame of the dominant Rossby wave, $\psi_{\text{pert}}(x, y, t)$ is periodic, or quasi-periodic in time. In general, one can think of the dimensional streamfunction consisting of a wave packet comprised with a finite or infinite number of Rossby waves. If limiting attention to countable waves, it would have the form

$$\psi_{k'l'}(x', y', t') = \sum_{k'} \sum_{l'} \varepsilon'_{kl} \sin\left[k' \left(x' - c'_{kl} t'\right)\right] \sin\left[l' y'\right] \tag{15}$$

in which the wavespeed of each mode (k', l') obeys

$$c'_{kl} = -\frac{\beta'}{(k'^2 + l'^2)} \tag{16}$$

for dynamical consistency. The coefficients ε'_{kl} are assumed small in comparison to A' in thinking of this as a *disturbance* on the dominant wave whose transport characteristics are shown in Figure 1. The sum in (15) may be over a finite number of wavenumbers (k', l'), or an infinite number, and the 'smallness' of the coefficients can be set with the requirement

$$\sum_{k'} \sum_{l'} \left|\varepsilon'_{kl}\right| \ll A \,.$$

More general wave packets in which the wavenumbers can be varying *continuously*, consisting of a superposition of an uncountable number of Rossby waves, is also allowable. That is,

$$\psi_{k'l'}(x', y', t') = \int_{-\infty}^{\infty} \int_{-\infty}^{\infty} \varepsilon'(k, l') \sin\left[k' \left(x' - c'_{kl} t'\right)\right] \sin\left[l' y'\right] \, \mathrm{d}k' \mathrm{d}l' \tag{17}$$

where the wavespeeds satisfy (16)[2], and with requirements on the coefficient functions $\varepsilon'(k',l')$ to ensure that the improper integral (15) converges. Moreover, (17) must be a *perturbation* on the dominant streamfunction ψ_0'. These requirements can be combined by insisting on

$$\int_{-\infty}^{\infty}\int_{-\infty}^{\infty}\left|\varepsilon'(k',l')\right|\mathrm{d}k'\mathrm{d}l' \ll A'\,.$$

In either of the forms (15) or (17), the t'-dependence will not in general be periodic or quasi-periodic. Moreover, the possibility of dealing with wave packets such as these is a first step to determining the flux occurring due to more stochastic perturbations, for example by choosing the εs from an appropriate random distribution.

Next, the same nondimensional transformation of coordinates, as given by (5) needs to be applied to the disturbance streamfunction. This will result in fluid parcel trajectories being described by

$$\frac{dx}{dt} = -\frac{\partial\psi}{\partial y} \quad , \quad \frac{dy}{dt} = \frac{\partial\psi}{\partial x} \tag{18}$$

with nondimensional streamfunction

$$\psi(x,y,t) = \psi_0(x,y) + \psi_{\mathrm{pert}}(x,y,t)\,. \tag{19}$$

and PV

$$q(x,y,t) = \nabla_0^2\psi(x,y,t) + f_0 - cy\,. \tag{20}$$

It is worth reiterating that the nondimensional disturbance streamfunction $\psi_{\mathrm{pert}}(x,y,t)$ obtained from (15) or (17) will have arbitrary t-dependence. Now, the quantification of the flux of fluid and potential vorticity occurring across Γ in Figure 1 is a nontrivial exercise given that the barrier breaks up into *two* different entities: a stable manifold *and* an unstable manifold, which do *not* coincide in general. They may intersect at infinitely many times, finitely many times, or even not at all. Moreover, these structures *will be moving with time*. The 'flow barrier' therefore consists of a region in which these stable and unstable manifolds intermingle. It is indeed not an impermeable flow barrier (unlike in Figure 1), but a 'barrier-region' across which transport *does* occur between the jet and the eddy. *Defining* what transport means in this context requires usage of recently developed dynamical systems methods, as are outlined in Section 2.2.

2.2. Fluid and potential vorticity flux

In unsteady flow situations, the unambiguous flux barrier Γ in Figure 1 breaks apart, into a separate stable and an unstable manifold. These need not coincide, and typically will exhibit complicated intersections when viewed at any time. The fact that the stable and unstable manifolds are themselves moving with time makes the identification of a 'flux' doubly difficult. This section will outline an emerging viewpoint on characterizing the flux (both fluid flux and PV flux) which:

- Allows for the disturbance to have *any* time-variation;
- Explicitly quantifies the flux as a function of time;
- Does not care whether manifolds intersect zero times, a finite number of times, or an infinite number of times; and
- Works for compressible two-dimensional flows[3].

---

[2] The wavenumber $(k',l') = (0,0)$ is disallowed, since there is no well-defined wavespeed c_{kl}' in (16) for this specific wavenumber.

[3] Geophysical fluid might need to satisfy *volume* preservation, and so when observing behavior on two-dimensional sheets (e.g., isopycnals), area-preservation need not be satisfied since the isopycnals can compress towards one another.

Since this viewpoint may be new to some, more details of this (including how it generalizes the concept of Poincaré maps and lobe dynamics) are presented in Appendix A for the interested reader. However, here a very brief overview of how fluid and PV flux can be thought of in a time-dependent sense, while respecting the Lagrangian nature of the problem, will be outlined.

Consider first *fluid* flux. Under the influence of the unsteady disturbance, the unstable manifold emanating from **a** in Figure 1 persists, but now as the *time-varying* unstable manifold of a specialized trajectory $\mathbf{a}(t)$ which moves around while continuing to lie on $y = 0$ near to **a**. This trajectory shall be referred to as an *anchoring trajectory* since the manifold is anchored to this[4]. A picture of this, at a time t, could possibly be like Figure 2(a), where the unstable manifold is shown in red. The claim now is that the unstable manifold of $\mathbf{a}(t)$ is a flow separator between the eddy and the jet in *backward time*. To see why this is so, consider two fluid parcels on the two sides of the unstable manifold, and imagine what happens to them in backward time. Eventually, at some time t_1, say, they will get close to $\mathbf{a}(t_1)$, and then they will move further apart (indeed, exponentially so) due to the presence of the stable manifold of $\mathbf{a}(t)$ along $y = 0$. One parcel gets pushed into the jet while the other unequivocally gets pushed into the eddy. Similarly, **b** perturbs to an anchoring trajectory $\mathbf{b}(t)$ whose stable manifold is a flow separator between the eddy and the jet in *forward time*. The trouble now is that these stable and unstable manifolds may intersect (or not) in many ways, and therefore quantifying a flux seems difficult. In typical chaotic situations, there will be infinitely many intersections, and thus the question is how one can obtain a computable definition for the *transfer of fluid between the eddy and the jet* when there is no longer any impermeable barrier to quantify flux across, the intersection region is highly complicated, and everything is changing with time.

One 'obvious' approach might be to think of using an Eulerian definition of flux across Γ. Such an Eulerian flux associated with (18) at any instance in time t is easily represented by

$$\text{Eulerian flux}\,(t) = \int_\Gamma \left\langle -\frac{\partial \psi_{\text{pert}}(x,y,t)}{\partial y}, \frac{\partial \psi_{\text{pert}}(x,y,t)}{\partial x} \right\rangle \cdot \hat{\mathbf{n}}(x,y)\, \sqrt{\mathrm{d}x^2 + \mathrm{d}y^2}\,, \tag{21}$$

where $\hat{\mathbf{n}}(x,y)$ is a unit normal vector to Γ at each location. This is not a good measure because of a variety of reasons. It is well-known that examining *Eulerian* characteristics fail in general to give proper *Lagrangian* information. This can be illustrated via several simple thought experiments. If the disturbance streamfunction retains the fact that the stable and unstable manifold coincide, then the definition should ensure that there is zero flux. However, if these coincide but at a slightly different location to that of Γ, (21) will give nonzero values. As another simple example, if the perturbed stable and unstable manifolds are both south of Γ in Figure 1, then (21) will be computing a flux from within the jet to within the jet, which is *not* what is of interest. Hence, a genuinely Lagrangian approach is necessary.

A simpleminded Lagrangian approach might be to compute the flux across a material curve, that is, a chain of particles, positioned for example on Γ, and then materially advected by the flow (18). The flux across this materially advected curve is *always zero*, since no fluid can cross the material curve. Thus, a 'pure Lagrangian' approach cannot capture flux between the eddy and the jet. A method which is able to capture the antecedents of fluid parcels (whether within or outside the eddy), and also the transfer across the 'barrier' which separates the eddy and the jet in the full flow (18), needs to be used.

Therefore, a Lagrangian method which takes into account the antecedents of fluid parcels needs to be used. The method builds on initial work by Haller and Poje [80] who introduced the idea of a 'gate,' and Miller et al [56] who used this to quantify PV flux near an island in an oceanic model. It is however the theoretical development of these concepts by Balasuriya [39,41,81] which leads to a well-defined formulation of the flux as a time-dependent entity. The crux of the idea is to simplify

[4] See Appendix A for a more rigorous understanding as to what this trajectory is.

Preprints (www.preprints.org) | NOT PEER-REVIEWED | Posted: 22 July 2016 doi:10.20944/preprints201607.0066.v1

Peer-reviewed version available at Fluids 2016, 1, 30; doi:10.3390/fluids1030030

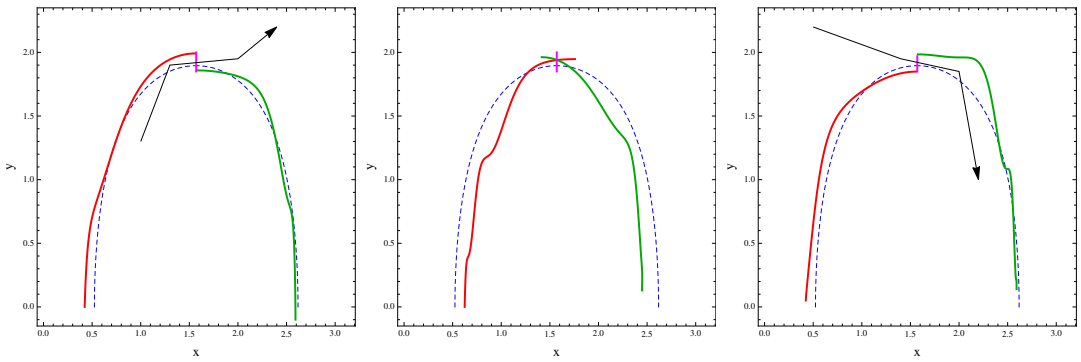

(a) positive flux (b) zero flux (c) negative flux

Figure 2. Intersection possibilities at three instances in time.

the potentially complicated intersection pattern by zeroing in specifically to the flux from inside to outside the eddy, by drawing a gate, a normal line to any chosen point on Γ. This is drawn in magenta in Figure 2, at the point $(\pi/2, \hat{y})$, the northernmost point of the dominant eddy. While an actual barrier between the eddy and the jet no longer exists, the unstable manifold emanating from $\mathbf{a}(t)$ is a barrier in backward time, and the stable manifold emanating from $\mathbf{b}(t)$ is a barrier in forward time. These manifolds are Lagrangian entities, which follow the flow. Capping these with the gate provides a 'nominal' flow barrier at any time. Thus, fluid can transition from 'inside the eddy' to 'outside the eddy' (i.e., 'in the jet') *only* by instantaneously crossing the gate. In other words, fluid particles can only transition from being inside the eddy in backward time to outside it in forward time (or vice versa) *if they cross the gate*. There are three qualitative possibilities for how the first intersection points of the unsteady stable and unstable manifolds meet on the gate, as shown in in Figure 2. Figure 2(a) indicates a situation in which fluid is instantaneously transporting from inside to outside the eddy; this shall be denoted as a *positive* fluid flux situation. Similarly, Figure 2(b) shows a *negative* flux scenario, and (b), in which the stable and unstable manifolds intersect exactly on the gate, has *zero* flux instantaneously. While potentially highly complicated intersections of the manifolds can occur *beyond* the gate, this knowledge is not necessary to determine the *flux* at any instance in time[5]. The flux from the eddy to the jet is therefore simply the flux through the gate. In this case, with the gate chosen to be at the northernmost point of Γ, the fluid flux is easily stated to be

$$\text{Fluid flux}\,(t) = \int_{y_s(t)}^{y_u(t)} \left(-\frac{\partial \psi(\frac{\pi}{2}, y, t)}{\partial y} \right) \mathrm{d}y\,, \tag{22}$$

where the gate lies between $y_s(t)$ and $y_u(t)$, i.e., the locations respectively at which the stable and unstable manifolds intersect the line $x = \pi/2$. Using (22) automatically imparts the correct sign for the fluid flux, since if $y_s(t) > y_u(t)$ (as shown in Figure 2(c)), the flux is negative. The fluid flux will have units of length squared per unit time, i.e., $\mathrm{m}^2\mathrm{s}^{-1}$ if measuring in SI units.

As time evolves, stable/unstable manifolds move, and thus so do the points $y_{s,u}(t)$. This gives the time-variation on the flux. Typically, if there are many intersections, there will be transitions between the different pictures in Figure 2(a) and (c) occurring as the intersection points 'flow through' the gate. The fluid flux defined in (22) *generalizes* well-known techniques such as lobe dynamics to arbitrary time-dependence. There are nice connections that can be made to these techniques, and are discussed in Appendix A.

---

[5] All intersection points will eventually move through the gate, and thus the method *will* take such intersections into account automatically when thinking of the flux's time-variation.

It is not only the amount of fluid that is transported across the Rossby eddy boundary that is of interest; so is the amount of PV transported. There are currently very few attempts of trying to quantify a potential vorticity flux across fluid boundaries which are internal to the fluid [56]. A simple extension of the idea of fluid flux, as argued in [39,41,52], can be used to quantify the transport of a tracer. The basic idea is that, once again, the flux can only occur through the gate. The amount of PV transported is determined by the PV carried by fluid parcels which cross the gate as shown in Figure 2. If $q(\pi/2, y, t)$ is the nondimensional PV of a particle located at $(\pi/2, y)$ (i.e., a general gate location) at time t, then the PV flux is defined by

$$\text{PV flux}\,(t) = \int_{y_s(t)}^{y_u(t)} q\left(\frac{\pi}{2}, y, t\right)\left(-\frac{\partial\psi(\frac{\pi}{2}, y, t)}{\partial y}\right) \mathrm{d}y\,. \tag{23}$$

This too is an instantaneous quantity, whose time-variation would quantify the time-varying nature of the potential vorticity transport from within the Rossby eddy to the stream. There is a slight difference in interpreting the sign of the potential vorticity flux as given in Figure 2; the sign of the flux as given there would be correct if all the fluid parcels crossing the gate had positive potential vorticity. Basically, the sign of q matters.

It should be noted that the development in this section is specifically associated with flux *across* Γ, that is, flux between the eddy and the jet. This is a much more specific issue that the commonly referred to 'potential vorticity flux' or 'eddy potential vorticity flux' which encapsulates the temporally-averaged covariance between the velocity and PV, or Lagrangian particle dispersion statistics [4,23,24,63]. In effect, the characterization here targets a specific aspect of the *inhomogeneous* [82] nature of PV mixing.

The flux of a tracer other than the PV, for example a concentration $c(x, y, t)$ of something (a pollutant such as oil [25], chlorophyll [83], temperature [84], etc) could *also* be quantified easily using this procedure: simply replace q in (23) with c. Therefore, the flux definitions given here are very general.

While the expressions (22) and (23) for the fluid and PV flux are simple, the difficulty comes in identifying the gate. That is, the stable and unstable manifolds for the perturbed flow (18) need to be known. This is a nontrivial exercise, since determining stable/unstable manifolds in unsteady flows is tricky even when the velocity is known explicitly[6]. Therefore, a method which can approximate these expressions to high accuracy (typically, to order-ε, where ε represents the relative size of the disturbance streamfunction in comparison to ψ_0) will be developed. In doing so, it helps to first consider a simple situation in which the disturbance consists of just one mode, in which case a fairly complete picture of the flux's behavior can be obtained.

3. Results

3.1. Formulas for flux

Given some *general* Rossby wave disturbations such as given by (15) or (17), the first issue is to provide a tool which assesses the flux generated by each particular mode. Picking any one of the dynamically-consistent Rossby wave with zonal and meridional wavenumbers k_1' and l_1' from (15) or (17), the disturbance streamfunction can be represented dimensionally by [3,6]

$$\psi_{k'l'}(x', y', t') = \varepsilon' \sin\left[k_1'\left(x' - c_1' t'\right)\right] \sin\left[l_1' y'\right] \tag{24}$$

---

[6] It is this difficulty which has led to the development of many proxies for the stable/unstable manifolds, such as ridges of FTLE fields [32,71], hyperbolic Lagrangian coherent structures [11], sharp transitions in various types of scalar fields generated from the flow using transfer operators [35], clustering [85] or averaging [25–27], etc.

where its wavespeed is $c_1' = -\beta'/(k_1'^2 + l_1'^2)$, and its amplitude is $\varepsilon' \ll A'$. In stating flux directions, $\varepsilon' > 0$ shall be assumed (if $\varepsilon' < 0$, the directions are reversed). There are many Rossby wave models in the literature which limit attention to this form of disturbance [45–47,57]. Under the nondimensionalization (5) and with the identification of the nondimensional parameters

$$k = \frac{k_1'}{k_0'} \quad , \quad l = \frac{l_1'}{l_0'} \quad , \quad \varepsilon = \frac{\varepsilon'}{A'} \quad , \quad c_{kl} = \frac{c_1'}{A' l_0'} , \tag{25}$$

it is possible to express the perturbed streamfunction in nondimensional form by

$$\psi_{\text{pert}}(x,y,t) = \psi_{kl}(x,y,t) = \varepsilon \sin\left[k\left(x + \left[c - c_{kl}\right]t\right)\right] \sin\left(ly\right) . \tag{26}$$

The full streamfunction associated with the flow (18) in the dimensionless coordinates in the moving frame is

$$\psi(x,y,t) = \sin\left(x\right)\sin\left(y\right) + cy + \varepsilon \sin\left[k(x + (c - c_{kl})t)\right] \sin\left(ly\right) , \tag{27}$$

where $\varepsilon \ll 1$. Examining the flow (18) for this streamfunction, the constant latitude line $y = 0$ is seen to be invariant under the flow for any choice of (k, l). Thus, the saddle points which were present when $\varepsilon = 0$ will maintain a y-value of zero, but since the system is now unsteady, they will wiggle around at this latitude. Thus, the unstable manifold will emanate from a (time-varying) point $\mathbf{a}(t)$ near $\mathbf{a}$, and the stable manifold from a point near $\mathbf{b}(t)$ near $\mathbf{b}$. Unlike when $\varepsilon = 0$ (when there was only the dominant Rossy wave), these stable and unstable manifolds *need not* coincide. The disruption of this unambiguous flow barrier (visible in magenta in Figure 1) will cause transport between the eddy and the jet.

It is worth stating that the nondimensional wavespeed can be written in the various forms

$$c_{kl} = -\frac{\beta'}{A' l_0' \left(k_1'^2 + l_1'^2\right)} = c\left(\frac{k_0'^2 + l_0'^2}{k_1'^2 + l_1'^2}\right) = c\left(\frac{k_0'^2 + l_0'^2}{k^2 k_0'^2 + l^2 l_0'^2}\right) . \tag{28}$$

The unsteadiness (genuine t-dependence) arises in the streamfunction (27) if

$$c \neq c_{kl} \quad \Longleftrightarrow \quad k_0'^2 + l_0'^2 \neq k_1'^2 + l_1'^2 . \tag{29}$$

The fluid and potential vorticity fluxes associated with the flow of (27) can be quantified very precisely. In Appendix B it is derived that the instantaneous signed fluid flux, as defined by (22), resulting from this second Rossby mode is

$$\text{Fluid Flux}\,(t) = \begin{cases} \varepsilon M_{kl}(t) + \mathcal{O}(\varepsilon^2) & \text{if } k_1'^2 + l_1'^2 \neq k_0'^2 + l_0'^2 \\ 0 & \text{if } k_1'^2 + l_1'^2 = k_0'^2 + l_0'^2 \end{cases} , \tag{30}$$

in which

$$M_{kl}(t) = A_{kl} \sin\left[k\left(\frac{\pi}{2} + (c - c_{kl})\,t\right) + \phi_{kl}\right] \tag{31}$$

for which explicit expressions for the amplitude A_{kl} and the phase ϕ_{kl} will be given momentarily. Given the complexity of the derivation (see Appendix B), this is a remarkably straightforward interpretation of the flux. If $c_{kl} \neq c$, it is sinusoidally varying with time, with a easily expressible [angular] frequency

$$\omega_{kl} = \left|k\left(c - c_{kl}\right)\right| . \tag{32}$$

It turns out that the flux can then be related nicely to 'classical' chaotic transport [51], including lobe areas, and the width of the chaotic zone. These are discussed in detail in Appendix A. A significant conclusion is that the amplitude A_{kl} is an excellent measure of the flux, irrespective of whether using the current time-varying viewpoint, areas of lobes, or width of the chaotic zone.

To give formulas for A_{kl} and ϕ_{kl}, the northernmost point of the Rossby eddy in Figure 1 needs to be computed. This occurs at $y = \hat{y}$, which is the solution to

$$\sin y = -cy \tag{33}$$

which lies in the domain $y \in (0, \pi)$. Equation (33) is transcendental and requires numerical evaluation. The formulas to be given from this point onwards assume that $-1 < c < 0$ (corresponding to $\beta' > 0$), in which case the Rossby wave travels as in Figure 1. Having determined $\hat{y}$ which satisfies (33), it is necessary to define the function

$$\xi(y) = \frac{\pi}{2} - \sin^{-1}\left(\frac{-cy}{\sin y}\right) + (c - c_{kl}) \int_y^{\hat{y}} \frac{\mathrm{d}u}{\sqrt{\sin^2 u - c^2 u^2}}\,, \tag{34}$$

and the integrals

$$I_s = \int_0^{\hat{y}} \cos\left[k\xi(y)\right] \cos\left[ly\right]\, \mathrm{d}y\,, \tag{35}$$

$$I_c = \int_0^{\hat{y}} \cos\left[k\xi(y)\right] \sin\left[ly\right] \frac{(y\cot y - 1)}{\sqrt{\sin^2 y - c^2 y^2}}\, \mathrm{d}y\,. \tag{36}$$

If $0 < c < 1$ (i.e., $\beta' < 0$), some slight adjustments to the above need to be made, to ensure that the principal branch of the $\sin^{-1}$ function does indeed capture what is required (in this case the flow directions of Figure 1 are reversed, and the location of the eddy also changes). In terms of the above quantities, the amplitude and the phase of the leading-order flux function (31) can be expressed by

$$A_{kl} = 2\sqrt{l^2 I_s^2 + c^2 k^2 I_c^2}\,, \tag{37}$$

$$\phi_{kl} = \tan^{-1}\frac{ckI_c}{lI_s}\,. \tag{38}$$

The derivation of these results is given in Appendix B.

What about the PV flux? The value of the PV of a fluid parcel flowing through the gate at a general time t is $\mathcal{O}(\varepsilon)$-close to the value of the unperturbed nondimensional PV (10) evaluated for a particle as it flows through the gate. Since the PV is identical for all points along the unperturbed heteroclinic (which is representible as a part of the level curve $q_0 = f_0$), this means that *all* particles which flow through the point $(\pi/2, \hat{y})$ will to leading-order carry a PV of f_0. The inclusion of the disturbance causes $\mathcal{O}(\varepsilon)$-perturbation to this, i.e.,

$$q(x, y, t)\Big|_{\text{gate}} = f_0 + \mathcal{O}(\varepsilon)\,, \tag{39}$$

where it shall be assumed that $f_0 \neq 0$. All the time-variation is luckily buried in the $\mathcal{O}(\varepsilon)$ term. Using (30), the PV flux (23) can be characterized by

$$\begin{aligned} \text{PV Flux}\,(t) &= \left[f_0 + \mathcal{O}(\varepsilon)\right]\left[\varepsilon M_{kl}(t) + \mathcal{O}(\varepsilon^2)\right] \\ &= \varepsilon f_0 M_{kl}(t) + \mathcal{O}(\varepsilon^2)\,. \end{aligned} \tag{40}$$

Following the same sign convention as for the fluid flux, the potential vorticity flux too is signed in the sense that potential vorticity flowing from the Rossby eddy to the main jet is positive. Moreover, it too is instantaneous.

An obvious observation from (40) is that the leading-order PV flux is simply the fluid flux multiplied by the constant f_0. Thus it too exhibits sinusoidal behaviour if $c_{kl} \neq c$, with amplitude $|f_0|\, A_{kl}$. Moreover, if $c_{kl} = c$—just as for the fluid flux—the PV flux also is zero. Therefore, in

Preprints (www.preprints.org) | NOT PEER-REVIEWED | Posted: 22 July 2016 doi:10.20944/preprints201607.0066.v1

Peer-reviewed version available at Fluids 2016, 1, 30; doi:10.3390/fluids1030030

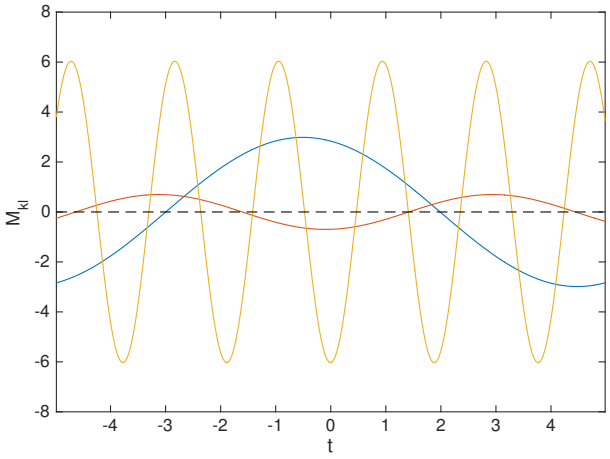

Figure 3. The instantaneous flux function (31) for $l = 1$, at several zonal wavenumber values: $k = 4$ [blue], 6 [red] and 18 [yellow].

obtaining the behaviour of the PV flux, *it suffices to simply examine the fluid flux*. One issue to note is that $f_0 < 0$ if in the southern hemisphere, indicating that PV flux is in the *opposite* direction to the fluid flux. (I.e., Negative PV is carried in the direction of the fluid transport.)

3.2. Optimal wavenumbers

Which modes are most effective in imparting flux between the jet and a flanking eddy? With the understanding that implications to the PV flux are buried within the results, attention will be focussed on the fluid flux. Examining the flux formula (30), it is clear that the primary parameter associated with the dominant Rossby wave which governs the flux is

$$c = -\frac{\beta'}{A' l_0' \left(k_0'^2 + l_0'^2\right)} \tag{41}$$

and hence the above combination of dimensional constants is important. The quantities (k_0', l_0') also impact on c_{kl} as shown in (28). The parameters A' and β' do not independently affect the flux. For numerical work, parameters associated with a midlatitude cyclone evolving in a background meandering atmospheric jet as studied by Oruba et al [9] will be used. Their Table 2 and Figure 5 indicate the values [9]

$$f_0' = 10^{-4}\,\mathrm{s}^{-1}\,,\ \beta' = 1.6\times 10^{-11}\,\mathrm{m}^{-1}\mathrm{s}^{-1}\,,\ \frac{2\pi}{k_0'} = 8000\,\mathrm{km}\,,\ \frac{2\pi}{l_0'} = 3000\,\mathrm{km}$$
$$\text{and } A' l_0' = 50\,\mathrm{ms}^{-1}\,. \tag{42}$$

These shall be the parameter values for the dominant Rossby wave used henceforth (unless specified otherwise), which give $c = -0.1868$. The nondimensional disturbance wavenumbers (k, l) are therefore scaled respectively by (k_0', l_0').

In Figure 3, the $\mathcal{O}(\varepsilon)$ term of the flux function (31) is displayed for several zonal wavenumbers k, at fixed meriodional wavenumber $l = 1$. The amplitude and the frequency vary as k changes. This picture displays one complete cycle for $k = 4$; fluid travels from the jet to the eddy (negative flux) for the first quarter period, and from the eddy to the jet (positive flux) for the middle half period, and then from the jet to the eddy in the final quarter. Thus, fluid sloshes back and forth once each during the pictured time. This causes some 'eddy fluid' to get entrained in the jet, and some 'jet fluid' to get entrained in the eddy. When $k = 6$, there are several more of these sloshing episodes, but the

Preprints (www.preprints.org) | NOT PEER-REVIEWED | Posted: 22 July 2016 doi:10.20944/preprints201607.0066.v1

Peer-reviewed version available at Fluids 2016, 1, 30; doi:10.3390/fluids1030030

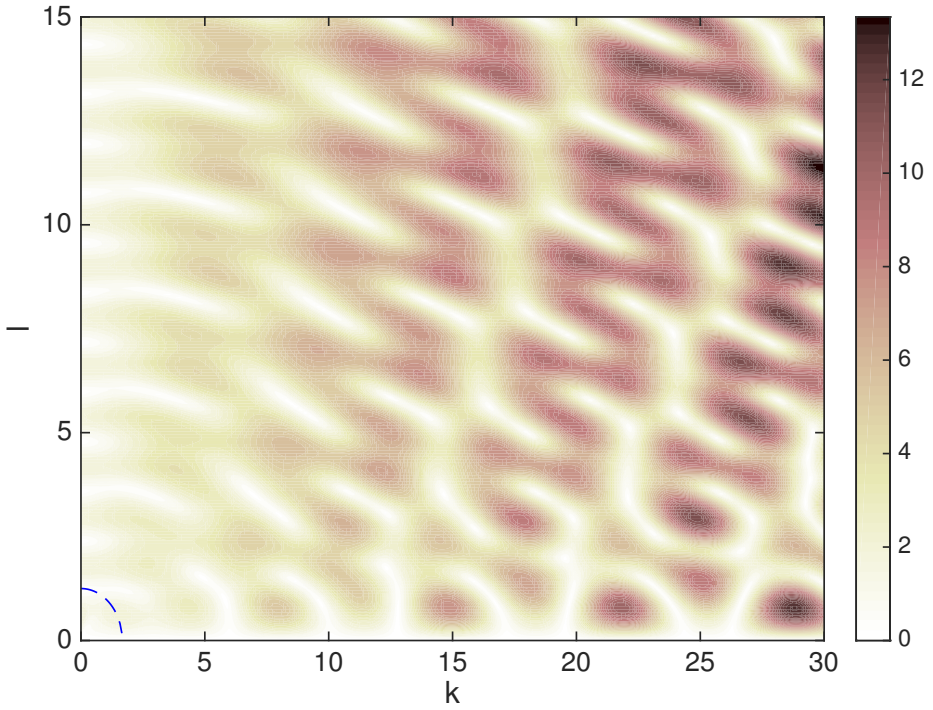

Figure 4. Dependence of amplitude A_{kl} on the wavenumbers (k,l), with the dashed blue curve corresponding to $c_{kl} = c$.

amount of fluid transferred (which is given by the area under the red curves in Figure 3 integrated between adjacent zeros), is smaller than the area under the blue curve. However, this is not the correct measure to use for flux, since these areas cross over different time-periods. As discussed in detail in Appendix A, it is A_{kl} which makes sense as a flux measure from both the continuous-time and the average flux viewpoints. From Figure 3, it is clear then that the blue curve ($k = 4$) has the greater amplitude than the red curve (with larger wavenumber $k = 6$), and thus can be taken to be associated with a larger flux. However, when $k = 18$ (the yellow curve), the amplitude is once again larger. This indicates that the flux amplitude, A_{kl}, does not have a monotonic behavior with respect to wavenumbers. Thus, Figure 3 is unable to tell us the zonal wavenumber corresponding to the maximum transport when $l = 1$. It is the amplitude A_{kl} which needs to be addressed.

Figure 4 shows the dependence of A_{kl} over a range of wavenumbers for the second Rossby mode. The dashed blue curve corresponds to wavenumbers at which $c_{kl} = c$, i.e., when the flux is actually zero. A broad region of (k,l)-space is examined, and to elucidate the behavior at small wavenumbers (long waves), a zoom in on this plot is shown in Figure 5. Smaller wavenumbers tend to have a small flux amplitude, indicating that disturbances with large spatial extent are not highly influential in causing eddy-jet transport. The picture for larger wavenumbers is more complex: there are wavenumber choices which generate very large flux (of size 14 at some locations in Figure 4, illustrating a resonance-type phenomena), and others where it is essentially zero. We see for example that a largest flux in the displayed wavenumber regime occurs if the secondary Rossby mode has $(k,l) \approx (22,1)$. The distribution is fairly irregular, and could not have been guessed at without having the theoretical methodology that has been developed, which provides an efficient method for perusing the (k,l) parameter space without having to do complicated Lagrangian advection numerics.

It was stated that the formula for A_{kl} needed adjustment if $\beta' < 0$, since then the undisturbed flow would not exactly be as in Figure 1 but will need a symmetric change, and the principal branch of the $\sin^{-1}$ function needed to be taken into account to deal with the adjusted locations of the anchoring

Preprints (www.preprints.org) | NOT PEER-REVIEWED | Posted: 22 July 2016 doi:10.20944/preprints201607.0066.v1

Peer-reviewed version available at Fluids 2016, 1, 30; doi:10.3390/fluids1030030

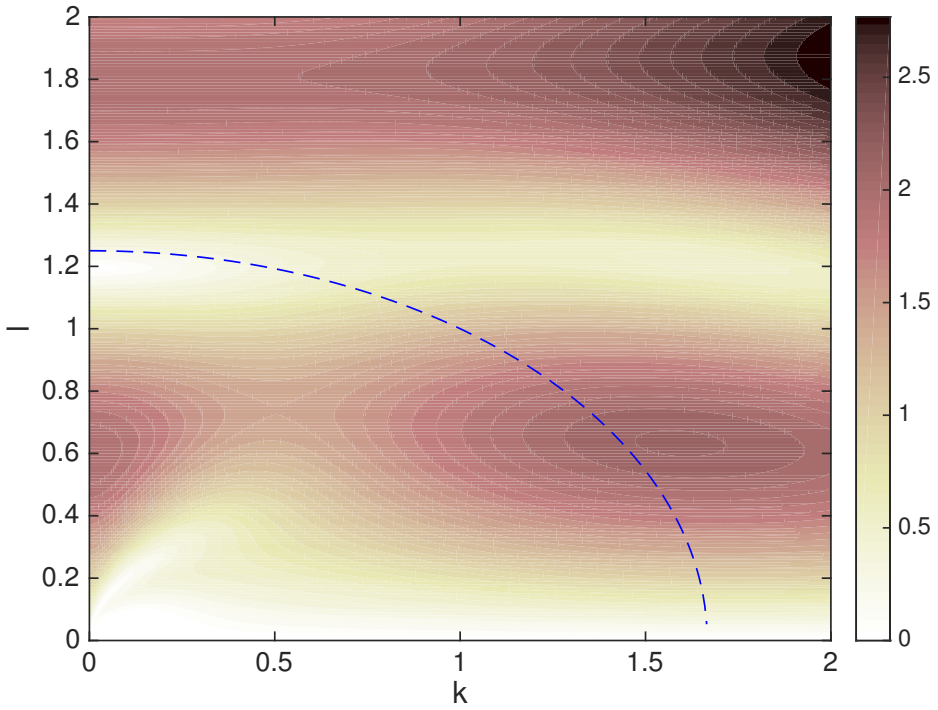

Figure 5. Zoom in to smaller wavenumbers in Figure 4.

trajectories. However, the adjustment is *symmetric* and not different in detail. Therefore, the computed A_{kl} for a particular c value should be exactly the same as for $-c$. This method is able to capture $\beta' < 0$ as well.

How well do the theoretical flux considerations obtained from Figure 4 match what actually happens? To analyze this, the stable and unstable manifolds for the disturbed system will be used. These are the organizing entities of the chaotic region, and their intersection pattern governs how complicated the mixing is. Figure 6 shows the numerically computed stable and unstable manifolds associated with four different values of the wavenumbers (k, l), chosen from Figs. 4 and 5 to have tiny, moderate, large and enormous flux amplitudes. Obtaining the manifolds numerically is nontrivial in this case since they are associated with a time-varying anchoring trajectory as opposed to a fixed point, and requires utilizing recent theoretical results [40,41]; a discussion of how these were obtained is given in Appendix C. Figure 6 captures the numerically obtained manifolds only up to a some finite length. All figures are produced by using $\varepsilon = 0.02$, a very small perturbation, and the A_{kl} value associated with each (k, l) pair is given in the captions. In (a), the manifolds fall virtually on top of each other; the interweaving is barely visible. Examining Figure 4, these correspond to wavenumbers in which the amplitude is very close to zero. In (b), there is a mildly discrenible difference between the two curves, and in (c), the lobe structure as anticipated by classical results [49,51]—but more irregular—is visible. Notice that the expectations of the lobes stretching and folding are in fact realized, and so chaotic transport will occur. Even for small ε, there is considerable mixing between the eddy and the jet. This lobe structure is *also* present in (a) and (b), but the deviations are too small to notice well.

A regime corresponding to a very dark patch in Figure 4, i.e., wavenumbers which our theory tell us correspond to very large transport, is examined in (d). Each manifold starts wiggling considerably when proceeding no great distance from its anchoring trajectory, resulting in a region of complicated intersections. It is worth noting that this intersection pattern does *not* conform to the 'classical' expectation of being like (c); there are many more wiggles, some lobe structures are very thin, and there are secondary intersections between the stable and unstable manifold. The strong folding (with

Preprints (www.preprints.org) | NOT PEER-REVIEWED | Posted: 22 July 2016 doi:10.20944/preprints201607.0066.v1

Peer-reviewed version available at Fluids 2016, 1, 30; doi:10.3390/fluids1030030

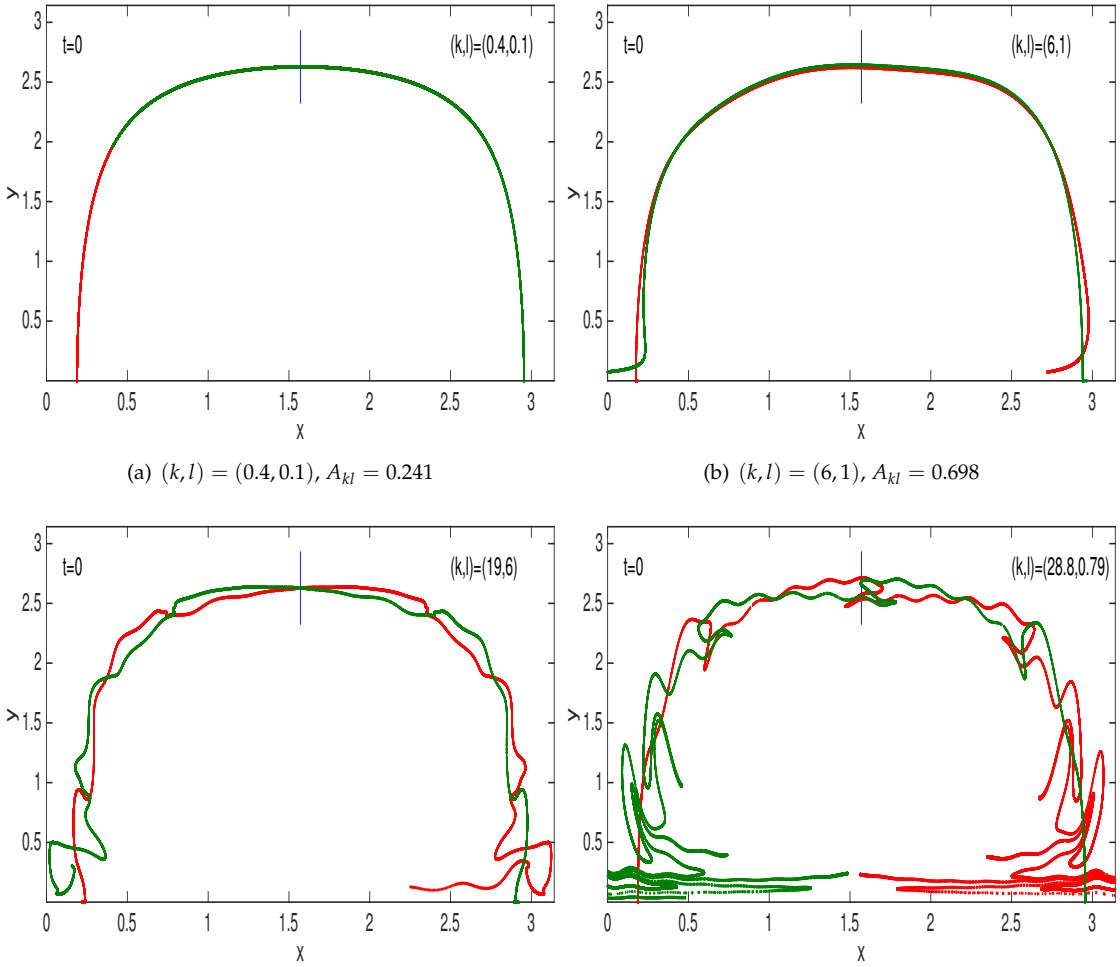

(a) $(k,l) = (0.4, 0.1)$, $A_{kl} = 0.241$

(b) $(k,l) = (6,1)$, $A_{kl} = 0.698$

(c) $(k,l) = (19,6)$, $A_{kl} = 6.025$

(d) $(k,l) = (28.8, 0.79)$, $A_{kl} = 12.766$

Figure 6. Numerically computed stable [green] and unstable [red] manifolds at $t = 0$ using $\varepsilon = 0.02$ and $c = -0.1868$.

the each manfold folding back on itself at some times) actually causes considerable additional mixing than that addressed here, since thin filaments are more susceptible to destruction via diffusion. There are several reasons for (d) not having the classically expected sinusoidal interweaving between the two manifolds. First, the expectation of the intersection pattern being sinusoidal along Γ is when *higher-order terms have been disregarded*. In this case, evidently, higher order terms become important. The reason for this is that A_{kl} is so large here that fluid parcels experience large excursions away from the previous eddy/jet boundary, and therefore their motion is impacted by velocities which are quite far from Γ. It is know [52] that *even in time-periodic situation*, the lobes created need not always have equal areas, as is apparent in (d). If, however, a much smaller ε were chosen, the excursions would be less, and the more well-behaved structure of (c) would be visible. However, the numerical calculations for (d) were also considerably more difficult than in the others, indicative of the strong chaotic mixing occurring within this manifold intersection region. In any case, since large A_{kl} indicates large excursions, using A_{kl} as a measure of how much fluid/PV is transported does remain legitimate.

At any frozen time (such as at the time $t = 0$ which is pictured), the instantaneous flux (fluid or PV) is obtainable by (22) or (23). The gate is shown by the blue line in all these panels, and as time progresses forward, say, all curves will 'flow to the right' resulting in the intersection patterns moving

Preprints (www.preprints.org) | NOT PEER-REVIEWED | Posted: 22 July 2016 doi:10.20944/preprints201607.0066.v1

Peer-reviewed version available at Fluids 2016, 1, 30; doi:10.3390/fluids1030030

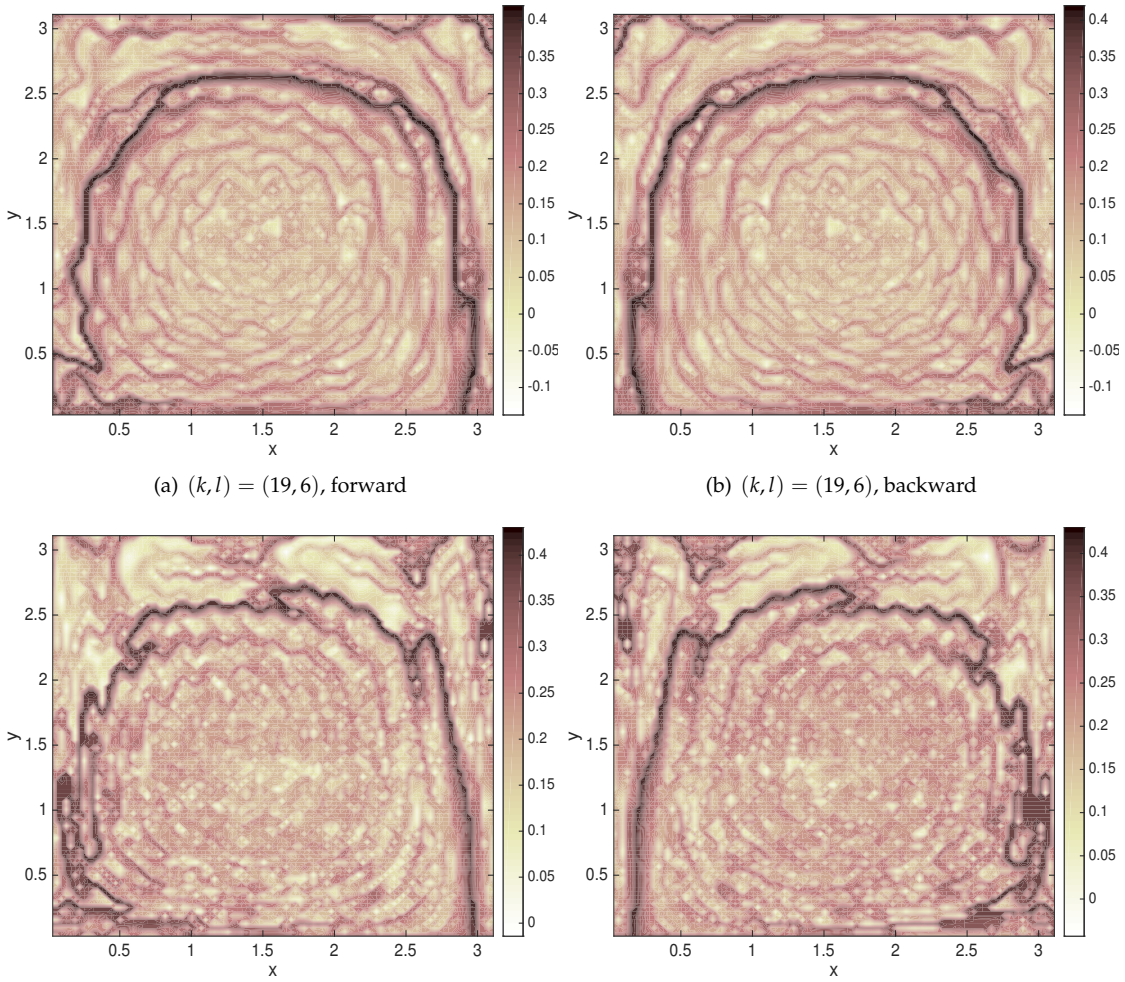

(a) $(k,l) = (19,6)$, forward

(b) $(k,l) = (19,6)$, backward

(c) $(k,l) = (28.8,0.79)$, forward

(d) $(k,l) = (28.8,0.79)$, backward

Figure 7. Forward and backward FTLE fields at $t = 0$ for identical parameter values as in Figure 6(c) and (d), with the choice of flow-time $T = 12$.

through the gate. The intersection patterns remains topologically preserved, but the actual shapes of the lobes can change during this procedure. After a time-period of $2\pi/\omega_{kl}$, a picture identical to Figure 6 will emerge, with the lobes having 'flowed rightwards' and now being exactly on top of one of the other lobes.

A further validation of these results is presented in Figure 7, which uses Finite-Time Lyapunov Exponent (FTLE) calculations. As argued by Samelson [12], from a practitioner's viewpoint, the FTLE can be thought of as the Finite-Time Lagrangian Strain (FTLS) incurred by a fluid element located at (x,y) at a specified time t, under the influence of the flow from the time t to $t+T$ (for forward FTLEs) or to $t-T$ for backward FTLEs. Balasuriya et al [32] rephrase Samelson's FTLS nomanclature as the Finite-Time Lagrangian *Stretching* experienced by an circular fluid parcel positioned at each location, after its Lagrangian evolution according to the flow over the specified time interval. Figure 7 shows the forward and backward FTLEs for several of the situations pictured in Figure 6. Under some nondegeneracy conditions [32], a strong ridge of the forward FTLE field is a proxy for the unstable manifold, while such a ridge for the backward FTLE is an indicator of the stable manifold [32,54,71]. The FTLE field will change according to the choice of T (the time of flow), for example picking up longer segments of the manifolds for larger T. The 'strongest' ridges (black curves) do fall on the stable/unstable manifolds as numerically obtained in Figure 6(c) and (d). This is visible if, for

example, comparing the green curve emanating from $\mathbf{b}(t)$ in Figure 6(c) with the ridge in Figure 7(a); the details of the behavior are spot on. This is also so for the other curves. The much more jagged form of the ridge in Figs. 7(c) and (d) in comparison with (a) and (b) provides an FTLE justification of greater transport between the eddy and the jet, once again validating the insight gained from Figure 4 on optimal wavenumbers.

FTLE computations (not shown) were also performed for situations in which $c_{kl} = c$, when the flux function, and thus the distance between the stable and unstable manifolds on the gate surface, should be zero at all times. The stable and unstable manifolds were seen to line up exactly on top of one another for this choice of disturbance wavenumbers.

Next, the sensitivity of the flux amplitude to the parameters of the main Rossby wave, given for all previous calculations by (42), is examined is Figure 8. These pictures are to be compared with Figure 4. In all cases, only *one* of the parameters in (42) is changed, with the other three being kept at the fixed values given in (42). The changes considered correspond respectively to a more poleward jet , the zonal jet speed halving, the zonal meanders having a spatial scale which is halved, and the meridional meander extent doubling. The maximum amplitude, as indicated by the colorbars on the left of each figure, does not change much. However, there are significant changes in the locations and distributions of the extrema. In (a) and (c), each zigzag structure of Figure 4 appears to have split apart into two distinct structures. Thus, for example, for eddy/jets further from the equation, it seems that there are many more values of (k,l) which locally maximize the fluid/PV flux, and that these have flux amplitudes which are not too different from each other. In (b) and (d), the maxima are more diffuse, indicating that if remaining within the (now larger) darker or lighter areas, changing (k,l) will not lead to much change. In other words, there is less sensitivity to (k,l). For example in (d), in which the meridional extent of the meanders is double that for Figure 4, there are very large areas in wavenumber space in which the flux is essentially zero. Therefore, the geometry, location and speed of the meandering jet impacts the amplitude map in nontrivial ways.

The ability to compute pictures such as Figure 8 quickly (each required just a couple of minutes of computation on a laptop computer) makes this a valuable tool. The alternative would be to search the (k,l) parameter space while for *each* wavenumber computing a flux-indicator (such as an FTLE field, stable/unstable manifolds, a mix-norm [72] or effective diffusivity [73–75] after simulating an advection-diffusion equation). This is numerically prohibitive, and would certainly not enable zeroing in to optimal wavenumbers in the way that Figs. 4, 5 and 8 does. As such, the methodology here provides a powerful new tool for seeking the most effective zonal and meridional wavenumbers for mixing.

3.3. Flux for wave packets

The flux formulation presented here has the advantage of *not* requiring time-periodicity. Therefore, it is able to deal with disturbance streamfunctions consisting not just of *one* mode, but infinitely many. That is, disturbances of the form (15) or (17) are fair game.

First, consider (15) which has a discrete set (potentially infinite) of values (k',l'). Nondimensionalizing each (k',l') according to (25) results in a set of nondimensional wavenumbers (k,l), each with its own nondimensional wavespeed c_{kl}. For each of these, the flux function is given by (30), where the ε can be replaced by ε_{kl}. Given the linearity of the Melnikov process in obtaining this as detailed in Appendix B, the full flux is therefore simply the linear superposition of all these. That is, for the disturbance streamfunction (15), the flux is given by

$$\text{Fluid flux}\,(t) = \sum_k \sum_l \varepsilon_{kl} A_{kl} \sin\left[k\left(\frac{\pi}{2} + (c - c_{kl})\,t\right) + \phi_{kl}\right] + \mathcal{O}(\varepsilon^2) \tag{43}$$

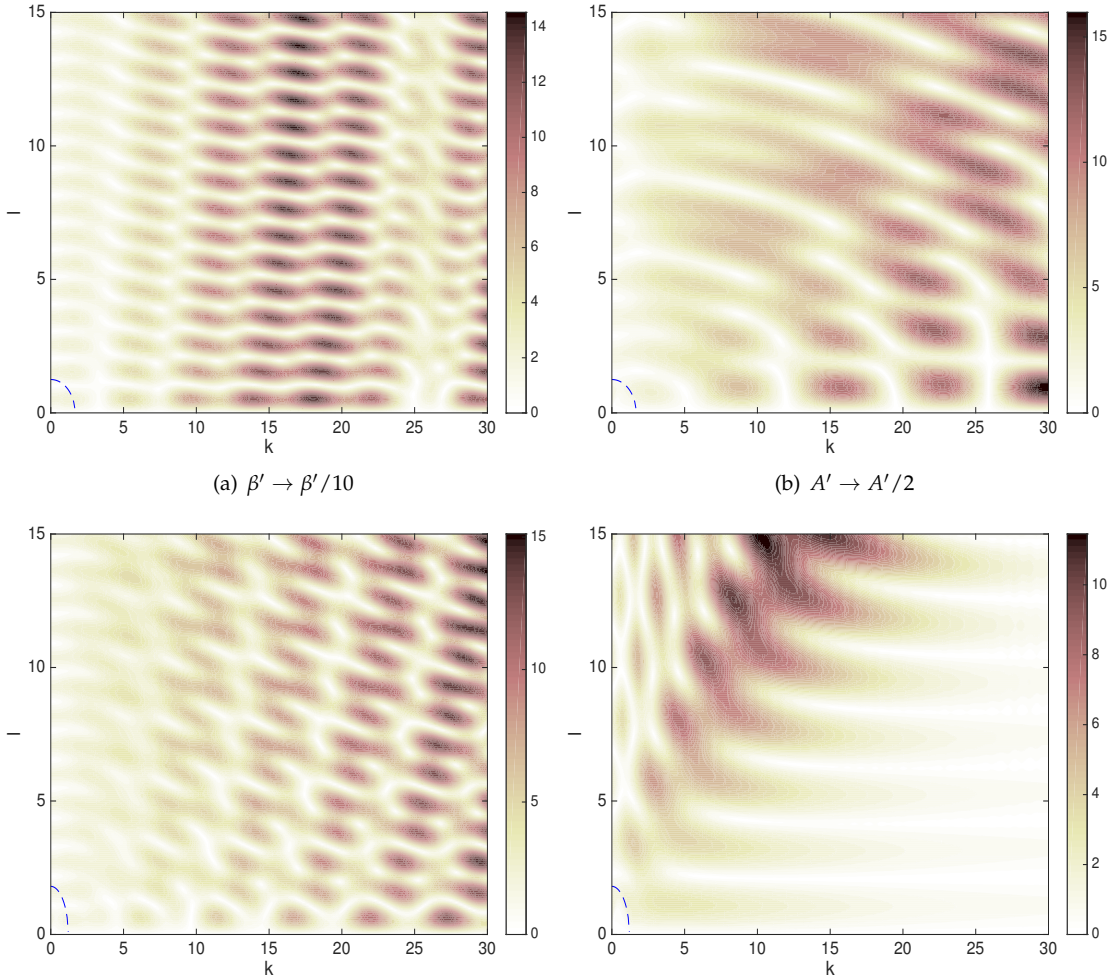

(a) $\beta' \to \beta'/10$ (b) $A' \to A'/2$

(c) $k_0' \to 2k_0'$ (d) $l_0' \to l_0'/2$

Figure 8. Changes to the flux amplitude when one of the parameters each in (42) is changed, with the the others kept fixed.

where an appropriate 'size' measure could be the L^1-norm

$$\varepsilon = \sum_k \sum_l |\varepsilon_{kl}| \ .$$

(The ε_{kl}s must be chosen so that the above converges, and is small.) The formula for A_{kl} and ϕ_{kl} is exactly as is given in (37) and (38). The PV flux would, by (40), simply be (43) mutiplied by f_0. Given the fact that the wavenumbers need not be commensurate, the flux (43) will in general *not* be periodic in time.

Figure 9(a) shows the time-varying flux computed for four wavenumbers

$$\begin{pmatrix} k \\ l \end{pmatrix} = \begin{pmatrix} -\ln 2 \\ 4 \end{pmatrix}, \begin{pmatrix} -\pi \\ 0.37 \end{pmatrix}, \begin{pmatrix} 23 \\ -\sqrt{7} \end{pmatrix} \text{ and } \begin{pmatrix} 5 \\ 5 \end{pmatrix}, \tag{44}$$

for the choice of ε_{kl}s for each of these (respectively) as specified. A complicated, time-aperiodic flux results from this, with transport both into and out of the eddy, with many fluctuations.

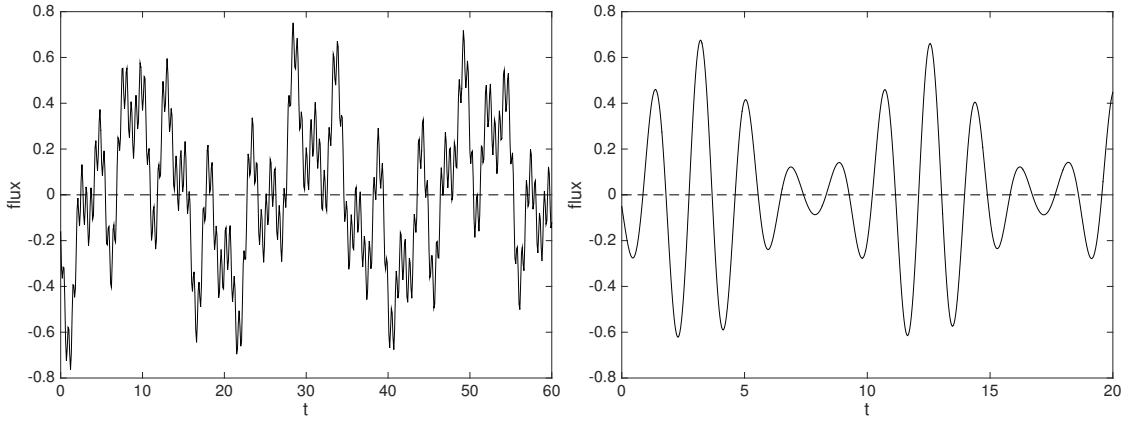

(a) $\varepsilon = (0.2, -0.07, 0.01, 0.13)$ (b) Continuous

Figure 9. The flux from the eddy to the jet for wave packet disturbances, computed using the discrete values (44) and the continuous values (46).

Next, consider the streamfunction (17), consisting of wavenumbers across a continuous spectrum. Once again, the same nondimensionalization as before, and the linearity, helps to write the fluid flux directly as

$$\text{Fluid flux}\,(t) = \int_{-\infty}^{\infty}\int_{-\infty}^{\infty} \varepsilon(k,l) A_{kl} \sin\left[k\left(\frac{\pi}{2} + (c - c_{kl})\,t\right) + \phi_{kl}\right] \mathrm{d}k\,\mathrm{d}l + \mathcal{O}(\varepsilon^2) \tag{45}$$

where

$$\varepsilon = \int_{-\infty}^{\infty}\int_{-\infty}^{\infty} |\varepsilon(k,l)|\;\mathrm{d}k\,\mathrm{d}l\,.$$

As an illustrative example, consider a disturbance streamfunction which consists of wavenumbers whose radial distance from $(k,l) = (7,1)$ is normally distributed, according to

$$\varepsilon(k,l) = 0.1\frac{1}{\sigma\sqrt{2\pi}} \exp\left[-\frac{(k-7)^2 + (l-1)^2}{2\sigma^2}\right]. \tag{46}$$

Figure 9(b) shows the resulting flux, computed using (45), for the choice of variance $\sigma = 1$. If $(k,l) = (7,1)$, the situation in Figs. 6(c) and 7(a,b), an essentially sinusoidal flux is to be essentially sinusoidal. The presence of nearby wavenumbers has changed this, but the regularity of the system is such that there appears to be periodicity. For less regular choices of $\varepsilon(k,l)$ (not pictured), the flux function turns out to be much less regular.

4. Discussion

The several simple examples presented here for wave packets is a taster for what is possible using the methodology that has been developed for assessing how Rossby-wave eddies interact with jets. In ongoing work, situations which are inspired by geophysical considerations, for example, Gaussian distributions around a collection of wavenumbers which are highly stable, is being pursued. Such an assessment would not be possible if using the 'classical' approach of Poincaré maps and lobe dynamics, since disturbance streamfunctions of this nature (and appearing in nature) are inevitably not time-periodic. As such, this paper presents a new theoretical tool which can be utilized for transport associated with Rossby waves in generic situations. For example, it is eminently possible in such situations for the stable and unstable manifolds to break apart such that they do *not* intersect [37,38,41], resulting in a unidirectional flux from the eddy to the jet (causing the eddy to eventually

deplete), or in the opposite direction (feeding the eddy from the jet)[7]. Many further investigations in this regard are possible, and called for, using these methods. For example, if data is available in a geophysical flow, its spatial Fourier transport can be used to identify the (k,l)-values which are present [83, e.g.] and the transport impact of this into the future might be estimated. Alternatively, if there are known stable wavenumbers [70, e.g.], the methdology could be applied directly to those.

The ability to determine wavenumbers which are associated with the highest (and least) transport without having to numerically advect particles for each particular wavenumber (k,l) is significant. This information is available directly from easily computable contour plots such as presented in Figure 4. The insight obtained from the contour plot was additionally validated using several other methods: numerical computation of the stable/unstable manifolds, and FTLE fields. Computing amplitude plots related to different jet geometries, locations and speeds (as shown for example in Figure 8) can provide a simple way of immediately viewing flux-maximizing and minimizing zonal and meridional wavenumbers for that particular dominant Rossby wave. This is in lieu of having to blindly perform numerics such as determining FTLEs, advecting (or advecting-diffusing) many particle trajectories under the flow and computing a mixing measure, etc. Since doing any of these for *each* (k,l) choice is computationally expensive, determining which (k,l)s are most effective for transport is not viable using such a process. As has been demonstrated, dramatically different amounts of transport (of fluid and potential vorticity) can occur when different (k,l)-disturbances are considered. A small investment of energy at the right spatial scales can engender very large transport; is it possible to harness this information for geophysical situations? Is there a relationship to the optimal wavenumbers for vorticity stirring power as developed by Barnes and Hartmann [7]?

This article has focussed on the streamfunctions as being governed specifically by Rossby wave dynamics, and for the eddy-jet geometry associated with a dominant Rossby wave. However, the methodology outlined here is adaptable to streamfunctions subject to different dynamical constraints, and different geometries which are nevertheless associated with an initially coincident stable and unstable manifold. It turns out that whenever the (size ε) disturbance streamfunction has time-sinusoidal dependence (whatever its spatial dependence might be), the flux across the nominal flow barrier will generically *always* take the form as given in (30), viz., $\varepsilon A_{kl} \sin\left[\omega_{kl} t + \phi_{kl}\right] + \mathcal{O}(\varepsilon^2)$. The *details* of the amplitude, frequency and phase will of course depend specifically on both the dominant and the disturbance streamfunction. Finding expressions for these in such cases will require a careful utilization of the geometry of the flow and the governing dynamics. Such expressions are no always easy to derive (witness the algebra in Appendix B for the specific Rossby wave situation), but can always be done in principle if full knowledge of the streamfunctions is available. Thus, it is certainly possible to modify this tool for determining optimal wavenumbers for fluid, potential vorticity, and possibly other tracer, flux, for *different* dynamics.

Acknowledgments: This work was partially supported by the Australian Research Council through grant FT130100484 of the Future Fellowship scheme.

Conflicts of Interest: The author declares no conflict of interest.

Appendix A. Relationship of flux definition to other methods

The flux definition (22), and in particular the form (30) obtained for the one-mode Rossby wave disturbance, has strong connections with a variety of other methods which are relevant to transport: lobe dynamics, lobe areas, and the width of the chaotic zone. This Appendix discusses these connections, and also outlines why the method—developed by Balasuriya [41,81]—is more general.

---

[7] Incompressibility is preserved in these situations by the fact that the stable and unstable manifolds move in time, for example by shrinking in towards the eddy center if the eddy is depleting.

Relationship to relative positioning of manifolds at each time: The flux formula (22), in the situation in which the disturbance is small, has a connection with the width of the chaotic zone. This is because flux occurs when the distance between $y_s(t)$ and $y_u(t)$ is large, and exactly this distance can be thought of as the width of the zone. Moreover, there is a dichotomy: viewing the width as a function of time at fixed gate location (which is the viewpoint here), is equivalent to thinking of the width as a function of gate location at fixed time [41,51]. The reason for this is that any intersection patterns which exist at a fixed time, will eventually have to move through a fixed gate when time is evolved. To state this more precisely, let ℓ be a signed arclength along Γ, chosen symmetrically such that the northernmost point of Γ, $(\pi/2, \hat{y})$ has $\ell = 0$, and $\ell < 0$ for $x < \pi/2$. Then, the displacement between the stable and the unstable manifold at a location ℓ, at time t, measured in the direction normal to Γ, can be represented by [41,86]

$$\text{Width}(\ell, t) = \frac{\varepsilon M_{kl}\left(t - \tau(\ell)\right)}{|\nabla \psi_0\left(\ell\right)|} + \mathcal{O}(\varepsilon^2)\,. \tag{47}$$

Here, $\tau(\ell)$ is the time at which a fluid element at $(\pi/2, \hat{y})$ at time zero (i.e., $\tau(0) = 0$) passes through a point on Γ with arclength parametrization ℓ, if flowing according to the the unperturbed flow (6) (see Balasuriya [41] for more details). The quantity M_{kl} in (47) is called a *Melnikov function* [41,49, 51,79,87,88], which has been used previously in the geophysical context [37,44,46,47]. For the *specific* single-mode disturbance discussed in Section 3.2, M_{kl} has the form given in (31), and is sinusoidal. (In general, under wave packet disturbances, it would have general time-dependence.) This implies that for $c_{kl} \neq c$, if viewing the stable/unstable manifolds at a fixed time t, there are infinitely many intersection between them because of M_{kl}'s sinusoidal behavior. Since they occur along Γ which has finite length, these intersection points accumulate towards the left and right endpoints (there are infinitely many of them, approaching these points arbitrarily closely). Moreover, $|\nabla \psi_0| \to 0$ in approaching these points, which means that width increases without bound. The region between adjacent intersections, i.e., lobes, are therefore closely positioned along Γ in these limits, and exhibit stretching in the transverse direction.

Relationship to chaotic transport: The condition $c_{kl} \neq c$ is equivalent to that stated for the flux to be nonzero in (30). In this case, M_{kl} is genuinely sinusoidal. This means it has infinitely many zeros. In view of the dichotomy discussed previously, if considering the picture at fixed time, this implies that the stable and unstable manifolds intersect infinitely often. Determining a zero of a Melnikov function in this way is one of the few approaches for *proving* that a system has chaotic transport [46,47, e.g.]. The focus in these articles was to prove the system was chaotic, which occurs when the Melnikov function has simple zeros in time-periodic flows. Technically, however, this furnishes a proof of chaos only in the *homoclinic* instance in which the two anchoring points are the same; in this case each manifold can be established to wrap around the homoclinic loop, intersecting the other manifold infinitely many times, and re-enter a region arbitrarily close to itself once again. This is a crucial ingredient in the proof of the Smale-Birkhoff theorem [79], one of few tools for proving the existence of chaotic transport. Since this situation is of a *heteroclinic* manifold, with $\mathbf{a}(t)$ and $\mathbf{b}(t)$ being diffferent, the Smale-Birkhoff theorem does not directly apply. In practice, though, the fact that the form (31) implies infinitely many intersections between the stable and unstable manifolds usually *does* result in chaotic transport between the eddy and the jet. This is because the intersection regions between them (the lobes) must stretch without bound when approaching the ends according to (47), and the confinement of these lobes which is ensured by the fact that the line $y = 0$ is invariant for the streamfunction (26). Thus, 'stretching' and 'folding' do occur in this situation, with intersection regions eventually forced to re-enter areas from which they left.

In the case of time-sinusoidal perturbations, in which the lobe-dynamics approach is valid, the lobes 'move through' the gate region as time evolves. This results in the flux function (22) itself being time-sinusoidal; indeed, more can be said [39,81]. There would then be a pulsation of fluid into and subsequently out of, the eddy, during one cycle (corresponding exactly to the sine function being

positive over the first half-cycle and negative over the next half-cycle), with this process repeating time-sinusoidally. For the sake or argument, suppose that the first half-cycle of this process is like Figure 2(a), with fluid passing from the eddy to the jet. One can think of the fluid passing through as 'filling a balloon,' with the process stopping when the flux becomes zero, i.e., Figure 2(b). The fluid which has 'filled the balloon' which has now passed from the eddy to the jet, consists of a fluid area which is *exactly* the area of the lobe if a lobe-dynamics viewpoint is adopted. During the second half of the cycle, the flux would be in the opposite direction, as pictured in Figure 2(c). In this duration, fluid fills out a lobe (which closes off when the stable and unstable manifolds once again meet exactly on the gate, at the end of the second half-cycle of this process) which intrudes from the jet to the eddy. This too has the same area. Thus, during one cycle, a lobe of fluid will go from the eddy to the jet, and another lobe (of the same area) will go from the jet to the eddy. This corresponds exactly to the two lobes which cross the pseudoseparatrix if using the classical lobe dynamics and turnstile approach [49,51]. Now, in this case, quite a lot more happens: these lobes travel down towards the anchoring trajectories which are wobbling around near **a** and **b**, experiencing elongation in the direction of the *opposite* manifolds emanating from these points along the line $y = 0$. Since also confined to be above this constant latitude, these lobes inside the eddy fold once they have elongated sufficiently to be once again in the zone of influence of the other anchoring trajectory. The 'stretching and folding' as they traverse the boundary region between the eddy and the jet leads to chaotic mixing. Thus, this is the fundamental mechanics which creates the well-known chaotic mixing between the eddy and the jet due to time-sinusoidal perturbations [49,51], whose *inception* is quantified by the flux (22).

Relationship to lobe areas: If $c_{kl} \neq c$, the amplitude A_{kl} has a relationship to the lobes generated when viewing the perturbed system in terms of a Poincaré map in the standard approach. Such lobes have equal areas, and the area of each lobe can be obtained by integrating the flux function between adjacent zeros [39,52], which in this case gives

$$\text{Lobe Area} = \frac{2\,|\varepsilon|\,A_{kl}}{\omega_{kl}} + \mathcal{O}(\varepsilon^2) == \frac{2\,|\varepsilon|\,A_{kl}}{|k(c-c_{kl})|} + \mathcal{O}(\varepsilon^2)\,. \tag{48}$$

Lobe areas typically increase with smaller k due to the presence of the k in the denominator of (48); the implied conclusion might initially be that transport always increases with decreasing wavenumber. This is a spurious, since there is a time-scale associated with the transport of a lobe. If using the turnstile approach to transport, one lobe will be transported from the eddy to the jet, while another (equal sized) lobe of fluid will transport in the opposite direction from the jet to the eddy, during one iteration of the Poincaré map [49,51]. Since the Poincaré map has period $2\pi/\omega_{kl}$, the average flux (lobe area divided by $2\pi/\omega_{kl}$) is more appropriate [50]. Examining (48), this is simply proportional to A_{kl}.

Different gate location: What if the gate were chosen at a different location? In this case, it can be shown [39,41] that the leading-order flux function $M_{kl}(t)$ simply acquires a translation. In other words, this can be accomodated by a shift in the value of the phase ϕ_{kl}. Importantly, this has no bearing on the amplitude A_{kl}.

A measure of fluid flux: In view of the above discussion, the amplitude of the flux function, A_{kl} is proposed as an appropriate quantifier of the time-varying flux. This makes sense from (31), with the added observation that it is independent of the location at which the gate was positioned. Moreover, it arises naturally from the concept of the average flux, while explicitly accounting for the time-variation in a sensible way. Thus, A_{kl} is an excellent flux measure, consistent with either the lobe dynamics and average flux approach, or the continuous-time approach used here, if $c_{kl} \neq c$.

What if $c_{kl} = c$***?*** Then, the disturbance has no unsteadiness, and so an initial conclusion that can be reached is that flux function is independent of time. If it is a non-zero constant, this means that the stable and unstable manifolds do not intersect. This would allow for a channel to open up, and uni-directional flux will occur between the eddy and the jet (in one direction, depending on this sign of this constant). Uni-directional flux can certainly happen in incompressible

geophysically-relevant flows, e.g., Kelvin-Stuart cats-eyes flows [37,41], or in kinematical eddies [38], but in these situations there is dissipation of potential vorticity due to diffusion or viscosity, and hence the flow is unsteady. This allows for incompressibility to be preserved in the system despite the uni-directional leaking of fluid (from inside the eddy, say), by the stable/unstable manifolds which bound the eddy getting closer and thereby enclosing lesser area as time progresses. *In the case examined in this paper*, however, the full flow is also steady, and therefore having such a channel open up would violate incompressibility. Therefore, if $c_{kl} = c$, the fluid flux must be zero; that is, the stable and unstable manifolds, which may move from their initial locations, do so in such a fashion as to still coincide. This is the reason why the flux is stated as being zero in (30) when the disturbance wavenumbers obey $k_1'^2 + l_1'^2 = k_0'^2 + l_0'^2$.

Time-periodicity is not necessary: The theoretical approach due to Rom-Kedar et al [49] was the first to provide a method for quantifying a flux in unsteady flows, due to the intersection of stable and unstable manifolds. This, however, relies on the velocity field being *time-periodic*, which allows for the definition of a *Poincaré map* P which simply strobes the flow at the period of the velocity [49,51,79]. Fixed points of P, and their stable and unstable manifolds, are then the focus. Their intersections creates *lobes*, and the impact of P on these lobes (i.e., the idea of *lobe dynamics*) gives insight into transport occurring over each time-period. In their classical picture, Rom-Kedar et al [49] show that the area of a lobe can be used as a transport measure, and in their case the lobes all have equal areas to make this unambiguous. Considerably more details on this are available in the book by Wiggins [51], and geophysical applications are plentiful [3,20,45–47,53].

The approach discussed in Section 2.2 generalizes this to general time-variation, as will be necessary for Rossby wave packets. There is then no preferred time period to sample the flow at, denying the opportunity of using a map P. One might try to use different Ps for different times or examine quasiperiodic flows to attempt to retain these ideas [57,59], but having a genuinely time-varying approach would be more powerful. Thus, instead of thinking of fixed points of a map, the points to which stable and unstable manifolds are anchored will be thought of in a time-varying way. So $\mathbf{a}(t)$ is a time-varying entity to which is attached a stable manifold. It turns out that $\mathbf{a}(t)$—previously referred to loosely as a specialized or anchoring trajectory—needs to be defined as a *hyperbolic trajectory*, which is associated with the concept of an exponential dichotomy [41,89]. This is difficult to use in general to *find* hyperbolic trajectories, though techniques which work under some circumstances exist [86,90]. However, the point is that a flux, as a genuinely time-varying entity which encapsulates the amount of fluid transferred per unit time, is the most reasonable thing to define.

Lobes are not necessary: The classical approach [49,51] requires there to be lobes present, created through intersecting stable and unstable manifolds. Moreover, to use a lobe area as a measure of transport, it is necessary that these lobes have equal areas. In contrast, the time-varying approach detailed in Section 2.2 does not require the stable and unstable manifolds to intersect at all. If they do not intersect—which is a distinct possibility when including the effects of dissipation in geophysical flows [37,38,41])—there are no lobes at all, and hence no 'lobe dynamics.' On the other hand, a lack of intersection makes perfect sense from the perspective of Figure 2: this implies a uni-directional flux, either from the eddy to the jet, or from the jet to the eddy. The instantaneous flux may change with time, but its *sign* does not.

It is also possible that there are a *finite* number of intersections between the stable and the unstable manifold. If so, how is lobe dynamics to be thought of? Which lobes get transferred? At what time? Again, the time-continuous approach completely avoids these difficulties.

Compressibility: The flux definition (22) is still legitimate even if the fluid were compressible. The only change that needs to be done is the replacement of $-\partial\psi/\partial y$ with the zonal velocity, whatever it happens to be. The issue is that if the fluid were compressible there would no longer be a streamfunction ψ that describes the velocity; however, the flux definition remains legitimate with the

(compressible) velocity inserted instead [41]. However, its usage in the compressible case requires a generalization of the standard Melnikov function [41,86].

The Melnikov function and flux: A pleasing theoretical issue of the instantaneous flux was developed by Balasuriya [39,81]: this flux, as a time-varying quantity which specifically measures the amount of fluid which is transported across per unit time, can be characterized to leading-order in ε exactly by a dynamical-systems tool called the *Melnikov function* (for fluids applications, see [38,44,46,47,49], for theory, see [41,51,79,87]). The argument of the Melnikov function relates precisely to time, and it is precisely this which appears in (30) and (31). Thus, unlike in the quantification of lobe areas which requires an *integral* of the Melnikov function [49–51], the Melnikov function *by itself* can be used to quantify the flux as a function of time [39,81]. The quantity $M_{kl}(t)$ is exactly a Melnikov function, as are the expressions (43) and (45) for non-sinusoidal situations. This works under general time-dependence and also compressibility [41].

Appendix B. Derivation of formula for A_{kl}

There is a nice formula for the amplitude A_{kl} for the Melnikov function $M_{kl}(t)$, using Fourier transforms [41,52], but this requires knowing the formula for the fluid trajectory $(\bar{x}(\tau), \bar{y}(\tau))$ along Γ according to the flow (6) which went through $(\pi/2, \hat{y})$ at time $\tau = 0$. This can only be defined implicitly, so an alternative will be used.

The formula for $M_{kl}(t)$ in (31) is based on the development outlined by Balasuriya [39,41], building also on prior results [81,86]. It first requires information on how a fluid parcel would flow on the unperturbed flow barrier, Γ, visible in Figure 1. This corresponds to a contour $\psi_0(x,y) = 0$, and so its coordinates obey

$$\sin x = -\frac{cy}{\sin y}$$

where it is recalled that $-1 < c < 0$. Thus the x-coordinate on Γ can be written

$$x(y) = \begin{cases} \sin^{-1}\left(\frac{-cy}{\sin y}\right) & \text{if } x \leq \pi/2 \\ \pi - \sin^{-1}\left(\frac{-cy}{\sin y}\right) & \text{if } x > \pi/2 \end{cases} . \tag{49}$$

The x-coordinate of the saddle point at the left is therefore obtained by taking the limit $y \to 0^+$, yielding $\sin^{-1}(-c)$, and similarly the right saddle point has x-coordinate $\pi - \sin^{-1}(-c)$. The northernmost point $(\pi/2, \hat{y})$ on Γ, from (49), then must satisfy (33). Now, from (6), if $x < \pi/2$,

$$\frac{dy}{dt} = \cos x \sin y = \sqrt{1 - \left(\frac{-cy}{\sin y}\right)^2}\, \sin y = \sqrt{\sin^2 y - c^2 y^2}\,,$$

where the positive root is chosen since $\sin x > 0$. Set $t = 0$ when $y = \hat{y}$. Then the time-variation along Γ as a function of y is must be given by

$$\tau(y) = \begin{cases} \int_{\hat{y}}^{y} \frac{\mathrm{d}u}{\sqrt{\sin^2 u - c^2 u}} & \text{if } x \leq \pi/2 \ (\tau \leq 0) \\ -\int_{\hat{y}}^{y} \frac{\mathrm{d}u}{\sqrt{\sin^2 u - c^2 u}} & \text{if } x > \pi/2 \ (\tau > 0) \end{cases} . \tag{50}$$

Consider a point with (signed) arclength parametrization ℓ on Γ, chosen such that $\ell = 0$ at $(\pi/2, \hat{y})$. Then, from equation (19) in Theorem 3 by Balasuriya [39], the width (measured from the stable to the unstable manifold, in the direction of $-\nabla\psi_0(\ell)$ at a location ℓ on Γ), can be represented by

$$\text{Width}(\ell, t) = \varepsilon \frac{\tilde{M}(\ell, t)}{|\nabla \psi_0(\ell)|} + \mathcal{O}(\varepsilon^2)\,, \tag{51}$$

where

$$\tilde{M}(\ell,t) = \int_\Gamma \mathbf{g}\left(\tau(\ell'), t+\tau(\ell')-\tau(\ell)\right)\cdot\hat{\mathbf{n}}(\ell')\,\mathrm{d}\ell'\,.$$

Here, $\mathbf{g}$ is the perturbing velocity, $\hat{\mathbf{n}}$ is the unit normal vector to Γ obtained by rotating the velocity vector by $\pi/2$ in the counter-clockwise direction, and $\tau(\ell)$ is the time-value, as in (50), at each location. Equation (51) represents a *signed width*, positive if the vector from the stable to the unstable manifold drawn at ℓ is in the same direction as $\hat{\mathbf{n}}$ and negative otherwise. Under the definition

$$M_{kl}(t) = \int_\Gamma \mathbf{g}\left(\tau(\ell'), t+\tau(\ell')\right)\cdot\hat{\mathbf{n}}(\ell')\,\mathrm{d}\ell'\,, \tag{52}$$

$\tilde{M}(\ell,t)$ can be replaced by $M_{kl}(t-\tau(\ell))$ in (51), thereby arriving at (47). Next, the fluid flux associated with positioning a gate at $\ell = 0$ is given by

$$\text{Fluid flux}(t) = (\text{Width}(0,t))\ (|\nabla\psi_0(0)| + \mathcal{O}(\varepsilon)) = \varepsilon M_{kl}(t) + \mathcal{O}(\varepsilon^2)\,,$$

where the first equality is because the speed at $(\pi/2,\hat{y})$ for the unperturbed flow is $|\nabla\psi_0|$, and thus all points in its vicinity—in particular on the gate—get modified by a $\mathcal{O}(\varepsilon)$ term when the disturbance is included. Therefore, (30) has been derived.

The next step is to work with the expression (52) and obtain the much more straightforward characterization (31). The disturbance velocity is, from (18) and (27),

$$\mathbf{g}(x,y,t) = \begin{pmatrix} -l\sin\left[k\left(x+(c-c_{kl})t\right)\right]\cos\left[ly\right] \\ k\cos\left[k\left(x+(c-c_{kl})t\right)\right]\sin\left[ly\right] \end{pmatrix}.$$

Given the different expressions for $x \le \pi/2$ and $x > \pi/2$ on Γ, it helps to think of Γ as consisting of Γ_- and Γ_+ in these respective domains, and to use the corresponding splitting $M_{kl}(t) = M_-(t) + M_+(t)$. On Γ_-, the normal vector in the direction of $\nabla\psi_0$ is

$$\mathbf{n} = \begin{pmatrix} \cos x\sin y \\ \sin x\cos y + c \end{pmatrix} = \begin{pmatrix} \sqrt{\sin^2 y - c^2y^2}, -c\left(y\cot y - 1\right) \end{pmatrix},$$

using (49). Thus the appropriate unit vector, pointing in this case from inside to outside the eddy, is

$$\hat{\mathbf{n}} = \frac{1}{\sqrt{\sin^2 y - c^2y^2 + c^2(y\cot y - 1)^2}}\begin{pmatrix} -\sqrt{\sin^2 y - c^2y^2}, c\left(y\cot y - 1\right) \end{pmatrix}.$$

Thus,

$$\mathbf{g}\cdot\hat{\mathbf{n}} = \frac{l\sin k\lambda\cos ly\sqrt{\sin^2 y - c^2y^2} + ck\cos k\lambda\sin ly\left(y\cot y - 1\right)}{\sqrt{\sin^2 y - c^2y^2 + c^2(y\cot y - 1)^2}}$$

where the shorthand

$$\lambda = x + (c - c_{kl})\,t$$

for a quantity that depends on both x (which itself depends on y via (49)) and time t, is used. However, to use (52), integration with respect to the arclength parameter ℓ is needed. On Γ_-, the differential elements are related via

$$\mathrm{d}\ell = \left(\sqrt{\left(\frac{dx}{dy}\right)^2 + 1}\right)\mathrm{d}y = \sqrt{\frac{c^2\left(y\cot y - 1\right)^2 + \sin^2 y - c^2y^2}{\sin^2 y - c^2y^2}}\,\mathrm{d}y\,,$$

where (49) has been used in simplifying. Therefore

$$\mathbf{g}\cdot\hat{\mathbf{n}}\,\mathrm{d}\ell = \left[l\sin k\lambda\cos ly + \frac{ck\cos k\lambda\sin ly\,(y\cot y-1)}{\sqrt{\sin^2 y - c^2y^2}}\right]\mathrm{d}y\,.$$

Combining all this information together, this means that the integral on Γ_- can be written as an integral in terms of y as

$$M_-(t) = \int_0^{\hat{y}} \left[l\sin k\xi_-\cos ly + \frac{ck\cos k\xi_-\sin ly\,(y\cot y-1)}{\sqrt{\sin^2 y - c^2y^2}}\right]\mathrm{d}y\,,$$

where

$$\xi_- = \xi_-(y,t) = \sin^{-1}\left(\frac{-cy}{\sin y}\right) + (c-c_{kl})\left(t + \int_{\hat{y}}^{y}\frac{\mathrm{d}u}{\sqrt{\sin^2 u - c^2u^2}}\right)$$

has both y and t dependence. A similar analysis, whose details will be skipped, enables the expression

$$M_+(t) = \int_0^{\hat{y}} \left[l\sin k\xi_+\cos ly + \frac{ck\cos k\xi_+\sin ly\,(y\cot y-1)}{\sqrt{\sin^2 y - c^2y^2}}\right]\mathrm{d}y\,,$$

where

$$\xi_+ = \xi_+(y,t) = \pi - \sin^{-1}\left(\frac{-cy}{\sin y}\right) + (c-c_{kl})\left(t - \int_{\hat{y}}^{y}\frac{\mathrm{d}u}{\sqrt{\sin^2 u - c^2u^2}}\right)\,.$$

The function $M_{kl}(t)$ is the sum of $M_-(t)$ and $M_+(t)$, which can be written alternatively as

$$M_{kl}(t) = M_s(t) + M_c(t)$$

where

$$M_s(t) = l\int_0^{\hat{y}} [\sin k\xi_- + \sin k\xi_+]\cos ly\,\mathrm{d}y$$

and

$$M_c(t) = ck\int_0^{\hat{y}} \frac{(\cos k\xi_- + \cos k\xi_+)\sin ly\,(y\cot y-1)}{\sqrt{\sin^2 y - c^2y^2}}\,\mathrm{d}y\,.$$

Using standard trigonometric addition formulas on the $\xi_\pm$ terms, a sine (respectively cosine) of the quantity $k\,(\pi/2 + (c-c_{kl})t)$ appears in each of M_s and M_c, and since independent of y, can be extracted from the integral. This enables M_{kl}, the sum of these two, to be written (using the definitions of I_s and I_c in (35) and (36)) as

$$\begin{aligned}
M_{kl}(t) &= 2lI_s\sin\left[k\left(\frac{\pi}{2}+(c-c_{kl})t\right)\right] + 2ckI_c\cos\left[k\left(\frac{\pi}{2}+(c-c_{kl})t\right)\right]\\
&= \sqrt{4l^2I_s^2+4c^2k^2I_c^2}\left\{\frac{2lI_s}{\sqrt{4l^2I_s^2+4c^2k^2I_c^2}}\sin\left[k\left(\frac{\pi}{2}+(c-c_{kl})t\right)\right]\right.\\
&\qquad \left. + \frac{2ckI_c}{\sqrt{4l^2I_s^2+4c^2k^2I_c^2}}\cos\left[k\left(\frac{\pi}{2}+(c-c_{kl})t\right)\right]\right\}\\
&= A_{kl}\sin\left[k\left(\frac{\pi}{2}+(c-c_{kl})t\right)+\phi_{kl}\right]\,,
\end{aligned}$$

using the definitions (37) and (38). This completes the derivation of the sinusoidal flux expression.

Appendix C. Numerical scheme for obtaining stable and unstable manifolds

There are many schemes available for numerically computing stable and unstable manifolds for *steady* flows, since in this case they are attached to an entity (e.g., a fixed point) which does not vary with time. This allows the scheme to start nearby (in some appropriately chosen way) of this *exactly known* entity. In this case, however, the stable and unstable manifolds are attached to hyperbolic (anchoring) trajectories which are varying with time, and whose location is *not* explicitly known. To deal with this difficulty, recent developments to approximate the hyperbolic trajectory's location [86,90] and direction of emanation of stable/unstable manifolds [40,41] will be used to advantage. Note that hyperbolic trajectory locations are *not* in general given by instantaneous stagnation points (see examples by Balasuriya [41]), necessitating a more refined approach.

Using Theorem 2.10 in [86], Theorem 2.1 in [40] or equation (2.5) in [90], the leading-order in ε location of the western (left) hyperbolic trajectory is representible as

$$\mathbf{a}(t) = \begin{pmatrix} \sin^{-1}(-c) - \dfrac{\varepsilon l \sin\left[k\left(\sin^{-1}(-c)+(c-c_{kl})t\right) - \tan^{-1}\frac{k(c-c_{kl})}{\sqrt{1-c^2}}\right]}{\sqrt{k^2(c-c_{kl})^2+\frac{1}{1-c^2}}} \\ 0 \end{pmatrix} + \mathcal{O}(\varepsilon^2)\,.$$

(The details of the algebra shall be skipped for brevity.) Similarly, the eastern hyperbolic trajectory is located approximately at

$$\mathbf{b}(t) = \begin{pmatrix} \pi - \sin^{-1}(-c) + \dfrac{\varepsilon l \sin\left[k\left(\pi-\sin^{-1}(-c)+(c-c_{kl})t\right) + \tan^{-1}\frac{k(c-c_{kl})}{\sqrt{1-c^2}}\right]}{\sqrt{k^2(c-c_{kl})^2+\frac{1}{1-c^2}}} \\ 0 \end{pmatrix} + \mathcal{O}(\varepsilon^2)\,.$$

The unstable manifold emanating from $\mathbf{a}(t)$ when $\varepsilon = 0$ (with no disturbance) points directly northward locally at the hyperbolic trajectory, which in this case is the fixed saddle point $\left(\sin^{-1}(-c), 0\right)$. The disturbance would in general give this northward emanation a time-dependent $\mathcal{O}(\varepsilon)$-variation, which is characterized by Theorem 2.2 in [40]. Using this, it turns out (calculations not shown) that the $\mathcal{O}(\varepsilon)$ change to this direction is zero. Thus, the unstable manifold, to leading-order in ε, will continue to emanate in the northward direction from the (time-varying) hyperbolic trajectory $\mathbf{a}(t)$. Similarly, the stable manifold emanating from $\mathbf{b}(t)$ will also continue to be in the northward direction locally at $\mathbf{b}(t)$.

Armed with this information, a numerical scheme can be devised for determining the unstable manifold attached to $\mathbf{a}(t)$, and the stable manifold attached to $\mathbf{b}(t)$, at any time t. Let T be a time-of-flow, and δ be a small parameter. To find the unstable manifold emanating from $\mathbf{a}(t)$, a line of particles emanating in the northward direction from $\mathbf{a}(t-T)$ up to a northward coordinate of δ is seeded. This is an approximation for the local unstable manifold at this instance in time, since the unstable manifold is known to point northwards to leading-order in ε. These particles are then advected forward by one-time step (i.e., to time $t - T + \Delta t$) according to (18) with the streamfunction (27), using a third-order Runge-Kutta scheme. At this next time-step, another line of particles, emanating northward from $\mathbf{a}(t - T + \Delta t)$ to a distance δ, is seeded. This is because this is the approximation for the local unstable manifold at this instance in time, which is different from what it was at time $t - T$. Then, *all* these particles are advected forward one more time-step, another line of particles is seeded at the new approximate location for the local unstable manifold, etc. This process is continued until the advection has progressed to time t. The particle locations will trace out the unstable manifold at time t. It is necessary to carefully choose how many particles to release at each time step to make sure that in the final result the points trace out the unstable manifold curve to the resolution required, while at the same time not unnecessarily oversampling the unstable

manifold curve. Oversampling can be a problem in that, since particles are introduced at every time step, their number can get astronomically large. The release of particles needs to be *nonuniform* over the time-steps. The sensitivity to the parameters δ and Δt need to also be checked before declaring satisfaction with the results. The parameter T determines how far to extend the unstable manifold.

Similarly, to find the stable manifold emanating from $\mathbf{b}(t)$, a line of particles is seeded from $\mathbf{b}(t+T)$ northwards to a distance of δ. The advection now occurs in the backward-time direction, but the details of the process are otherwise exactly as for the unstable manifold. Performing these numerical calculations leads to Figure 6.

Bibliography

1. Randall, D. *An introduction to the global circulation of the atmosphere*; Princeton University Press: Princeton, 2015.
2. Pedlosky, J. *Geophysical Fluids Dynamics*; Springer: New York, 1979.
3. Pierrehumbert, R. Chaotic mixing of tracer and vorticity by modulated travelling Rossby waves. *Geophys. Astrophys. Fluid Dyn.* **1991**, *58*, 285–319.
4. Mizuta, G. Role of Rossby waves in the broadening of an eastward jet. *J. Phys. Oceanography* **2012**, *42*, 476–494.
5. Graef, F. Free and forced Rossby normal modes in a rectangular gulf of arbitrary orientation. *Dyn. Atmos. Oceans* **2016**, *75*, 46–57.
6. Kiladis, G. Observations of Rossby waves linked to convection over the eastern tropical Pacific. *J. Atmos. Sci.* **1998**, *55*, 321–339.
7. Barnes, E.; Hartmann, D. Rossby wave scales, propagation, and variability of eddy-driven jets. *J. Atmos. Sci.* **2011**, *68*, 2893–2908.
8. Oruba, L.; Lapeyre, G.; Riviere, G. On the northward motion of midlatitude cyclones in a barotropic meadering jet. *J. Atmos. Sci.* **2012**, *69*, 1793–1810.
9. Oruba, L.; Lapeyre, G.; Riviere, G. On the poleward motion of midlatitude cyclones in a baroclinic meandering jet. *J. Atmos. Sci* **2013**, *70*, 2629–2649.
10. O'Rourke, A.; Vallis, G. Jet interaction and the influence of a minimum phase speed bound on the propagation of eddies. *J. Atmos. Sci.* **2013**, *70*, 2614–2628.
11. Haller, G. Lagrangian Coherent Structures. *Ann. Rev. Fluid Mech.* **2015**, *47*, 137–162.
12. Samelson, R. Lagrangian motion, coherent structures, and lines of persistent material strain. *Ann. Rev. Marine Sci.* **2013**, *5*, 137–163.
13. Rypina, I.; Pratt, L.; Pullen, J.; Levin, J.; Gordon, A. Chaotic advection in an archipelago. *J. Phys. Oceanography* **2010**, *40*, 1988–2006.
14. Tew Kai, E.; Rossi, V.; Sudre, J.; Weirmerskirch, H.; Lopez, C.; Hernandez-Garcia, E.; Marsac, F.; Garcon, V. Top marine predators track Lagrangian coherent structures. *Proc. Nat. Acad. Sci.* **2009**, *106*, 8245–8250.
15. Levy, M.; Jahn, O.; Dutkiewicz, S.; Follows, M.; d'Ovidio, F. The dynamical landscape of marine phytoplankton diversity. *J. Roy. Soc. Interface* **2015**, *12*, 20150481.
16. BozorgMagham, A.; Ross, S.; Schmale, D. Local finite-time Lyapunov exponent, local sampling and probabilistic source and destination regions. *Nonlin. Proc. Geophys.* **2015**, *22*, 663–677.
17. d'Ovidio, F.; Fernandez, V.; Hernandez-Garcia, E.; Lopez, C. Mixing structures in the Mediterranean sea from finite-size Lyapunov exponents. *Geophys. Res. Lett.* **2004**, *31*, L17203.
18. d'Ovidio, F.; Isern, J.; López, C.; Hernández-García, C.; García-Ladona, E. Comparison between Eulerian diagnostics and finite-size Lyapunov exponents computed from the altimetry in the Algerian basin. *Deep-Sea Res.* **2009**, *56*, 15–31.
19. Allshouse, M.; Peacock, T. Refining finite-time Lyapunov ridges and the challenges of classifying them. *Chaos* **2015**, *25*, 087410.
20. Ngan, K.; Shepherd, T. Chaotic mixing and transport in Rossby-wave critical layers. *J. Fluid Mech.* **1997**, *334*, 315–351.
21. Joseph, B.; Legras, B. Relation between kinematic boundaries, stirring and barriers for the Antarctic polar vortex. *J. Atmos. Sci.* **2002**, *59*, 1198–1212.

22. Prants, S.; Budyansky, M.; Ponomarev, V.; Uleysky, M. Lagrangian study of transport and mixing in a mesoscale eddy street. *Ocean Modelling* **2011**, *38*, 114–125.
23. Pratt, L.; Barkan, R.; Rypina, I. Scalar flux kinematics. *Fluids* **2016**, *in press*.
24. Rypina, I.; Kamenkovich, I.; Berloff, P.; Pratt, L. Eddy-induced particle dispersion in the near-surface north Atlantic. *J. Phys. Oceanography* **2012**, *42*, 2206–2227.
25. Mezić, I.; Loire, S.; Fonoberov, V.; Hogan, P. A new mixing diagnostic and Gulf oil spill movement. *Science* **2010**, *330*, 486–489.
26. Mancho, A.; Small, D.; Wiggins, S.; Ide, K. Computation of stable and unstable manifolds of hyperbolic trajectories in two-dimensional, aperiodically time-dependent vector fields. *Physica D* **2003**, *182*, 188–222.
27. Haller, G.; Hadjighasem, A.; Farazmand, M.; Huhn, F. Defining coherent vortices objectively from the vorticity. *J. Fluid Mech.* **2016**, *795*, 136–173.
28. Rypina, I.; Scott, S.; Pratt, L.; Brown, M. Investigating the connection between complexity of isolated trajectories and Lagrangian coherent structures. *Nonlin. Proc. Geophys.* **2011**, *18*, 977–987.
29. Allshouse, M.; Thiffeault, J.L. Detecting coherent structures using braids. *Physica D* **2012**, *241*, 95–105.
30. Budišić, M.; Thiffeault, J.L. Finite-time braiding exponents. *Chaos* **2015**, *25*, 087407.
31. Ma, T.; Bollt, E. Differential geometry perspective of shape coherence and curvature evolution by finite-time nonhyperbolic splitting. *SIAM J. Appl. Dyn. Sys.* **2014**, *13*, 1106–1136.
32. Balasuriya, S.; Kalampattel, R.; Ouellette, N. Hyperbolic neighborhoods as organizers of finite-time exponential stretching. *submitted* **2016**.
33. Froyland, G.; Horenkamp, C.; Rossi, V.; van Sebille, E. Studying an Agulhas ring's long-term pathway and decay with finite-time coherent sets. *Chaos* **2015**, *25*, 083119.
34. Froyland, G.; Stuart, R.; van Sebille, E. How well-connected is the surface of the ocean? *Chaos* **2014**, *24*, 0333126.
35. Froyland, G.; Padberg, K. Almost-invariant sets and invariant manifolds – connecting probabilistic and geometric descriptions of coherent structures in flows. *Physica D* **2009**, *238*, 1507–1523.
36. Ser-Giacomi, E.; Rossi, V.; López, C.; Hernández-García, E. Flow networks: a characterization of geophysical fluid transport. *Chaos* **2015**, *25*, 036404.
37. Balasuriya, S.; Jones, C.; Sandstede, B. Viscous perturbations of vorticity-conserving flows and separatrix splitting. *Nonlinearity* **1998**, *11*, 47–77.
38. Balasuriya, S.; Jones, C. Diffusive draining and growth of eddies. *Nonlin. Proc. Geophys.* **2001**, *8*, 241–251.
39. Balasuriya, S. Nonautonomous flows as open dynamical systems: characterising escape rates and time-varying boundaries. In *Ergodic Theory, Open Dynamics, and Coherent Structures*; Bahsoun, W.; Bose, C.; Froyland, G., Eds.; Springer, 2014; pp. 1–30.
40. Balasuriya, S. Local stable and unstable manifolds and their control in nonautonomous finite-time flows. *J. Nonlin. Sci.* **2016**, *26*, 895–927.
41. Balasuriya, S. *Melnikov methods for flow barriers and transport in unsteady flows*; in press, SIAM Press: Philadelphia, 2016.
42. Brown, M.; Samelson, R. Particle motion in vorticity-conserving two-dimensional incompressible flows. *Phys. Fluids* **1994**, *6*, 2875–2876.
43. Balasuriya, S. Gradient evolution for potential vorticity flows. *Nonlin. Proc. Geophys.* **2001**, *8*, 253–263.
44. Samelson, R. Fluid exchange across a meandering jet. *J. Phys. Oceanography* **1992**, *22*, 431–442.
45. del Castillo Negrete, D.; Morrison, P. Chaotic transport by Rossby waves in shear flow. *Phys. Fluids A* **1993**, *5*, 948–965.
46. Weiss, J.; Knobloch, E. Mass transport by modulated traveling waves. *Phys. Rev. A* **1989**, *40*, 2579–2589.
47. Knobloch, E.; Weiss, J. Chaotic advection by modulated traveling waves. *Phys. Rev. A* **1987**, *36*, 1522–1524.
48. Pratt, L.; Lozier, M.; Beliakova, N. Parcel trajectories in quasigeostrophic jets: neutral modes. *J. Phys. Oceanography* **1995**, *25*, 1451–1466.
49. Rom-Kedar, V.; Leonard, A.; Wiggins, S. An analytical study of transport, mixing and chaos in an unsteady vortical flow. *J. Fluid Mech.* **1990**, *214*, 347–394.
50. Rom-Kedar, V.; Poje, A. Universal properties of chaotic transport in the presence of diffusion. *Phys. Fluids* **1999**, *11*, 2044–2057.
51. Wiggins, S. *Chaotic Transport in Dynamical Systems*; Springer-Verlag: New York, 1992.

52. Balasuriya, S. Direct chaotic flux quantification in perturbed planar flows: general time-periodicity. *SIAM J. Appl. Dyn. Sys.* **2005**, *4*, 282–311.
53. Rypina, I.; Brown, M.; Kocak, H. Transport in an idealized three-gyre system with application to the Adriatic sea. *J. Phys. Oceanography* **2009**, *39*, 675–690.
54. Rypina, I.; Brown, M.; Beron-Vera, F.; Koak, H.; Olascoaga, M.; Udovydchenkov, I. On the Lagrangian dynamics of atmospheric zonal jets and the permeability of the stratospheric polar vortex. *J. Atmos. Sci.* **2007**, *64*, 3595–3610.
55. Prants, S.; Budyansky, M.; Uleysky, M. Chaotic mixing and transport in a meandering jet flow. *Chaos* **2006**, *16*, 033117.
56. Miller, P.; Pratt, L.; Helfrich, K.; Jones, C. Chaotic transport of mass and potential vorticity for an island recirculation. *J. Phys. Oceanography* **2002**, *32*, 80–102.
57. Malhotra, N.; Wiggins, S. Geometric structures, lobe dynamics, and Lagrangian transport in flows with aperiodic time-dependence, with applications to Rossby wave flow. *J. Nonlin. Sci.* **1998**, *8*, 401–456.
58. Mancho, A.; Hernández-Garcia, E.; Small, D.; Wiggins, S.; Fernández, V. Lagrangian transport through an ocean front in the northwestern Mediterranean sea. *J. Phys. Oceanography* **2008**, *28*, 1222–1237.
59. Ide, K.; Wiggins, S. Transport induced by mean-eddy interaction: I. Theory, and relation to Lagrangian lobe dynamics. *Commun, Nonlin. Sci. Numer. Simulat.* **2015**, *20*, 516–535.
60. Kamenkovich, V.; Kamenkovich, I. On the evolution of Rossby waves, generated by wind stress in a closed basin, incoporating total mass conservation. *Dyn. Atmos. Oceans* **1993**, *18*, 67–103.
61. Peacock, T.; Dabiri, J. Introduction to focus issue: Lagrangian Coherent Structures. *Chaos* **2010**, *20*, 017501.
62. Peacock, T.; Haller, G. Lagrangian Coherent Structures: the hidden skeleton of fluid flows. *Physics Today* **2013**, *66*, 41.
63. Berloff, P. Dynamically consistent parametrization of mesoscale eddies-Part II eddy fluxes and diffusivity from transient impulses. *Fluids* **2016**, *1*, 22.
64. Rogerson, A.; Miller, P.; Pratt, L.; Jones, C. Lagrangian motion and fluid exchange in a barotropic meandering jet. *J. Phys. Oceanography* **1999**, *29*, 2635–2655.
65. Shevchencko, I.; Berloff, P. Multi-layer quasi-geostrophic dynamics in eddy-resolving regimes. *Ocean Modelling* **2015**, *94*, 1–14.
66. Maddison, J.; Marshall, D.; Shipton, J. On the dynamical influence of ocean eddy potential vorticity fluxes. *Ocean Modelling* **2015**, *92*, 169–182.
67. Yang, H.; Wu, L.; Shantong, S.; Zhaohui, C. Low-frequency variability of monsoon-driven circulation with application to the South China sea. *J. Phys. Oceanography* **2015**, *45*, 1632–1650.
68. Enomoto, T.; Matsuda, Y. Rossby wavepacket propagation in a zonally-varying basic flow. *Tellus* **1999**, *51A*, 588–602.
69. Farrell, B. Optimal excitation of neutral Rossby waves. *J. Atmos. Sci.* **1988**, *45*, 163–180.
70. Balmforth, N.; Piccolo, C. The onset of meandering in a barotropic jet. *J. Fluid Mech.* **2001**, *449*, 85–114.
71. Shadden, S.; Lekien, F.; Marsden, J. Definition and properties of Lagrangian coherent structures from finite-time Lyapunov exponents in two-dimensional aperiodic flows. *Physica D* **2005**, *212*, 271–304.
72. Mathew, G.; Mezić, I.; Petzold, L. A multiscale measure for mixing. *Physica D* **2005**, *211*, 23–46.
73. Nakamura, N. Two-dimensional mixing, edge formation, and permeability diagnosed in area coordinates. *J. Atmos. Sci.* **1996**, *53*, 1524–1537.
74. Shuckburgh, E.; Haynes, P. Diagnosing transport and mixing using a tracer-based coordinate system. *Phys. Fluids* **2003**, *15*, 3342–3357.
75. Hendricks, E.; Schubert, W. Transport and mixing in idealized barotropic hurricane-like vortices. *Q. J. R. Meteorol. Soc.* **2009**, *135*, 1456–1470.
76. Rowe, S.; Hitchman, M. On the relationship between inertial instability, poleward momentum surges, and jet intensifications near midlatitude cyclones. *J. Atmos. Sci.* **2016**, *73*, 2299–2315.
77. Held, I.; Pierrehumbert, R.; Garner, S.; Swanson, K. Surface quasi-geostrophic dynamics. *J. Fluid Mech.* **1995**, *282*, 1–20.
78. Bower, A. A simple kinematic mechanism for mixing fluid across a meandering jet. *J. Phys. Oceanography* **1991**, *21*, 173–180.
79. Guckenheimer, J.; Holmes, P. *Nonlinear Oscillations, Dynamical Systems and Bifurcations of Vector Fields*; Springer: New York, 1983.

80. Haller, G.; Poje, A. Finite time transport in aperiodic flows. *Physica D* **1998**, *119*, 352–380.
81. Balasuriya, S. Cross-separatrix flux in time-aperiodic and time-impulsive flows. *Nonlinearity* **2006**, *19*, 282–311.
82. McIntyre, M. Potential vorticity. In *Encyclopedia of Atmospheric Science*, 2 ed.; North, G.; Zhang, F.; Pyle, J., Eds.; Elsevier, 2012.
83. Chelton, D.; Gaube, P.; Schlax, M.; Early, J.; Samelson, R. The influence of nonlinear mesoscale eddies on oceanic chlorophyll. *Science* **2011**, *334*, 328–332.
84. Gaultier, L.; Djath, B.; Verron, J.; Brankart, J.M.; Brasseur, P.; Melet, A. Inversion of submesoscale patterns from a high-resolution Solomon Sea model: Feasibility assessment. *J. Geophys. Res. Oceans* **2014**, *119*, 4520–4541.
85. Hadjighasem, A.; Karrasch, D.; Teramoto, H.; Haller, G. Spectral clustering approach to Lagrangian vortex detection. *Phys. Rev. E* **2016**, *93*, 063107.
86. Balasuriya, S. A tangential displacement theory for locating perturbed saddles and their manifolds. *SIAM J. Appl. Dyn. Sys.* **2011**, *10*, 1100–1126.
87. Melnikov, V.K. On the stability of the centre for time-periodic perturbations. *Trans. Moscow Math. Soc.* **1963**, *12*, 1–56.
88. Samelson, R.; Wiggins, S. *Lagrangian transport in geophysical jets and waves*; Interdisciplinary Applied Mathematics, Springer, 2006.
89. Coppel, W.A. *Dichotomies in Stability Theory*; Number 629 in Lecture Notes in Mathematics, Springer-Verlag: Berlin, 1978.
90. Balasuriya, S.; Padberg-Gehle, K. Controlling the unsteady analogue of saddle stagnation points. *SIAM J. Appl. Math.* **2013**, *73*, 1038–1057.